Master's Thesis

SOURCE IDENTIFICATION OF PM$_{10}$ AND SO$_2$ IN A MULTI-INDUSTRIAL CITY OF KOREA

Sang-Jin Lee

Department of Urban and Environmental Engineering

(Environmental Science and Engineering)

Graduate School of UNIST

2018

SOURCE IDENTIFICATION OF PM$_{10}$ AND SO$_2$ IN A MULTI-INDUSTRIAL CITY OF KOREA

Sang-Jin Lee

Department of Urban and Environmental Engineering

(Environmental Science and Engineering)

Graduate School of UNIST

SOURCE IDENTIFICATION OF PM$_{10}$ AND SO$_2$
IN A MULTI-INDUSTRIAL CITY OF KOREA

A thesis/dissertation

submitted to the Graduate School of UNIST

in partial fulfillment of the

requirements for the degree of

Master of Science

Sang-Jin Lee

7. 13. 2018 Month/Day/Year of submission
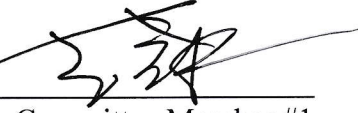
Approved by

Advisor

Sung-Duek Choi

SOURCE IDENTIFICATION OF PM_{10} AND SO_2 IN A MULTI-INDUSTRIAL CITY OF KOREA

Sang-Jin Lee

This certifies that the thesis of Sang-Jin Lee is approved.

7. 13. 2018 Month/Day/Year of submission

Advisor: Prof. Sung-Deuk Choi

Prof. Chang-Keun Song: Thesis Committee Member #1

Prof. Myong-In Lee: Thesis Committee Member #2

Abstract

Ulsan is the largest industrial city of South Korea. A large area of the city is covered by automobile, shipbuilding, petrochemical, and non-ferrous industrial complexes. Among criteria air pollutants (CAPs), particulate matters (PM) and sulfur dioxide (SO2) directly related to the main industries are major environmental concerns in Ulsan. Basically, the effect of local sources is crucial for these pollutants. Also, long-range atmospheric transport (LRAT) from China is an important source of CAPs, especially for PM10. However, there has been no studies dealing with LRAT and local pollution of CAPs together in Ulsan.

In this study, we collected and interpreted hourly data on CAPs measured at 14 automatic monitoring stations. The conditional bivariate probability function (CBPF), a receptor model, was used in order to identify local pollution sources of PM10 and SO2. An air dispersion model, California puff (CALPUFF), was also used to evaluate the influence of the industrial emissions by using 2012 Clean Air Policy Support System (CAPSS) data. The correlation analysis between the concentrations derived by CALPUFF and the monitoring data was conducted to identify the influence of local industrial sources. For LRAT of PM10, the potential source contribution function (PSCF) and cluster analysis of back-trajectories were performed. Totally, the monitoring data, modelling results, and back-trajectory data were derived at the hourly data set. These parameters were processed using statistical analysis, such as c-tree and random forest to assess the major sources between local and LRAT effects for each month.

The hourly data of PM10 showed the highest level in April and May and the lowest in August and December. Besides, the highest and the lowest concentrations of SO2 were observed in July and December, respectively. CBPF results indicated that the petrochemical industry and road traffic were the main local sources of PM10, whereas SO2 concentration was greatly influenced by the petrochemical industry. From CALPUFF results, both PM10 and SO2 were dispersed from the industrial areas to the residential areas in summer. The PSCF and cluster analysis results showed the potential LRAT sources of PM10 was china in spring. Lastly, the importance between the local and LRAT impacts in each month was identified by the statistical analysis. The local impacts of PM10 and SO2 were the largest in summer and decreased in winter. The LRAT of PM10 was observed when high levels of PM coming from China occurred in spring. This study can be a basis to identify the local and long-distance sources of CAPs in other cities.

Contents

List of Figures

List of Tables

I. INTRODUCTION

1.1 Particulate Matter

The particulate matters are mainly referred to as PM_{10} (Diameter less than 10) and $PM_{2.5}$ (Diameter less than 2.5) (Figure 1). $PM_{1.0}$ or less particle has also become an issue in recent. PM_{10} and $PM_{2.5}$ are classified as Criteria air pollutants (CAPs) including SO_2, NO_2, CO, O_3, Pb. Among the CAPs, PM_{10} was one of the major problems in East Asia since China was most PM_{10} sources (Toshihiko et al., 2002). The World Health Organization (WHO) has been providing air quality guidelines for PM_{10} and $PM_{2.5}$ since 1987. In 2013, the International Agency for Research on Cancer (IARC) classified the particulate matters as Group 1 carcinogens (WHO, 2013). In general, PM10 were also well known about causing acute effect like bronchoconstriction and chronic effects like asthma symptoms (Maji et al., 2017). Even the particulate matters affect the visible distance depending on the concentration. When the concentration is high, the light is scattered and absorbed by the fine dust, and the visible distance decreases. In addition, when the concentration increases in a high state to a humidity, contaminants in the atmosphere absorb moisture to generate secondary aerosols, and the visible distance is also decreased (Cheung et al., 2005).
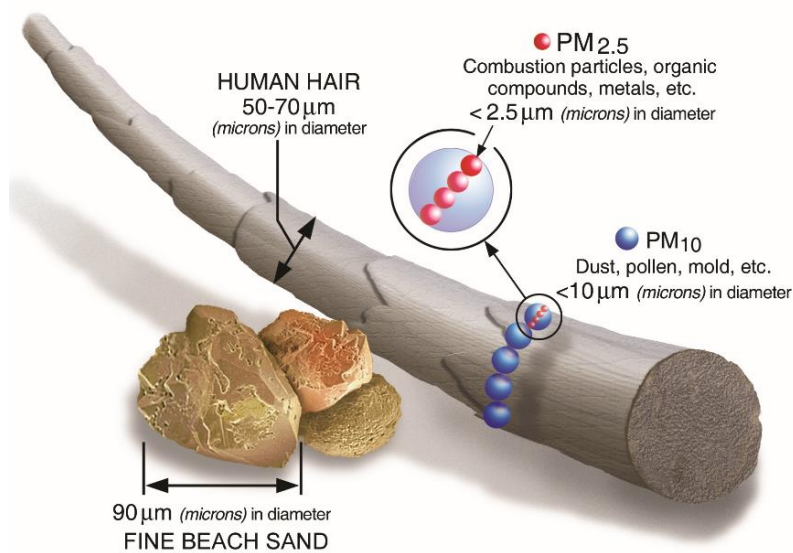
Figure 1. Definition and size of PM_{10} and $PM_{2.5}$ (EPA, 2015)

The sources of particulate matters are divided a natural source and an anthropogenic source. Natural sources are divided into primary particles directly discharged from soil, ocean, forest fire, and secondary particles generated through atmospheric chemical reactions. Examples of primary particles include dust, sea salt, and pollen from plants. Anthropogenic sources, like natural sources, are divided into primary and secondary particles. Primary particles are emitted directly from stationary and mobile sources, and secondary particles are generated by atmospheric chemical reactions (Goossens and Buck, 2011). Primary particles are mainly generated from power generation facilities, such as fossil fuel, coal, and petroleum combustion. In addition, they also emitted from manufacturing industry, vehicles, construction, waste treatment plant, and so on (Figure 2).
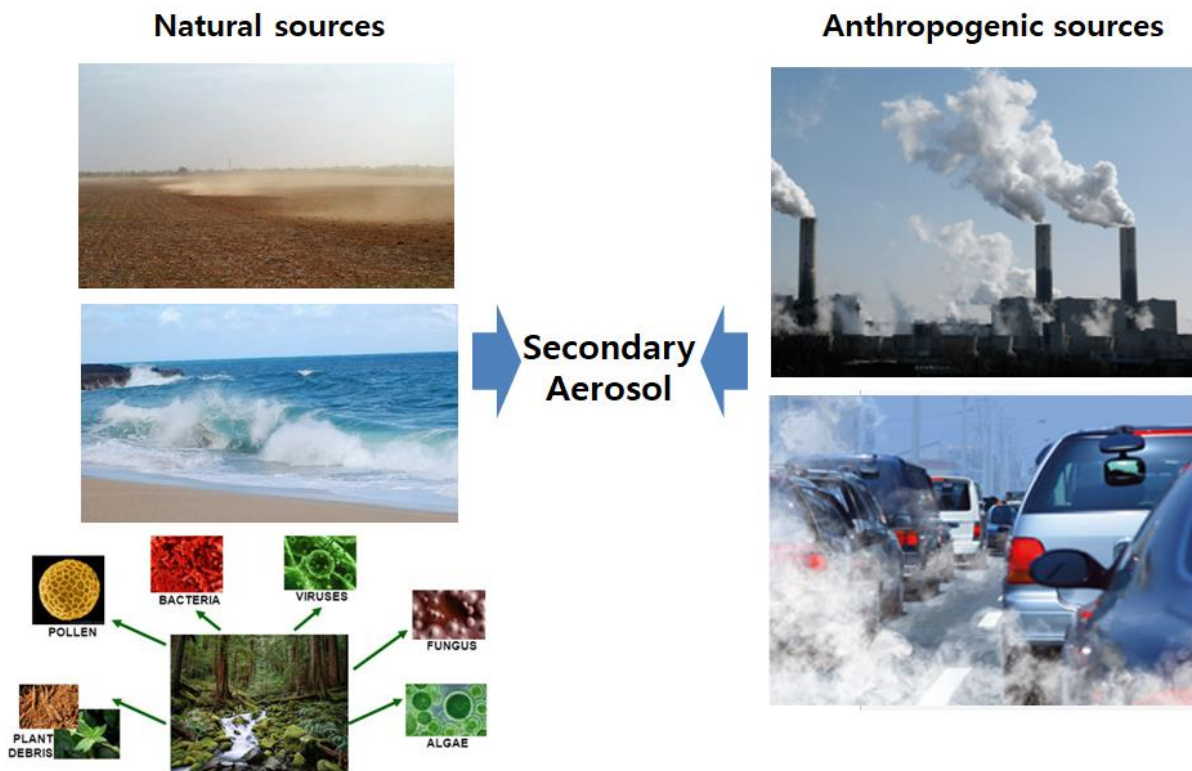
Figure 2. Natural and Anthropogenic sources of particulate matter

Secondary aerosols are generated through complicated reaction processes such as chemical reaction, adsorption, absorption (Kroll and Seinfeld, 2008). The major constituents are water-soluble ion components such as SO_4^{2+}, NO_3^-, NH_4^+, and organic substances. Secondary organic particles are also formed by the reaction of volatile organic compounds (VOCs) with highly reactive substances such as OH radical and O_3. The nitrogen oxides (NO, NO_2) generated in the combustion process react with O3

(HNO$_3$). The ammonia (NH$_3$) is reacted to generate ammonium nitrate (NH$_4$NO$_3$) which is a secondary particulate matter (Figure 3) (Lim and Ziemann, 2005).
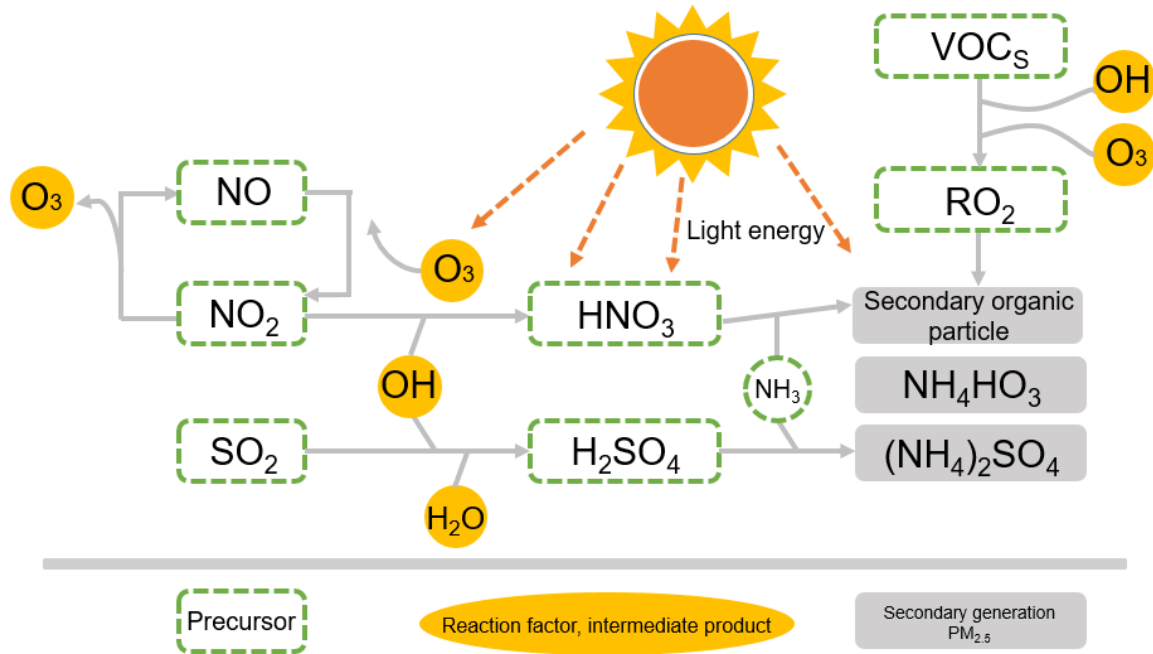
Figure 3. Principle of generating secondary particulate matters

PM$_{10}$ and PM$_{2.5}$ are considered in the world, so many countries regulate the standard concentrations of particulate matters in the air environment. The regulation level of both PM$_{10}$ and PM$_{2.5}$ deal with daily average concentration and annual average concentration. In Korea, the yearly standard level of PM10 is 50 μg/m^3, daily is 100 μg/m^3, and the case of PM$_{2.5}$ is 25 μg/m^3 of yearly and 50 μg/m^3 of daily. Comparing with Europe, Japan, Canada, USA and Austria, the standard level of regulation in Korea are relatively low. Hong Kong and China are only less regulated than Korea. In Korea, it is necessary to further improve the atmospheric environment and strengthen the regulation.

Table 1. The standards for particulate matter in atmosphere by countries

	PM_{10} ($\mu g/m^3$)		$PM_{2.5}$ ($\mu g/m^3$)	
	24 hours	Yearly	24 hours	Yearly
Korea	100	50	50	25
USA	150		35	12
Japan	100		35	15
Canada	25		15	
Australia	50		25	8
Hong Kong	100	50	75	35
China	150	70	75	35
UK	50	40		25
EU	50	40		25
WHO	50	20	25	10

1.2 Sulfur dioxide

Sulfur dioxide (SO_2) is well-known as typical air pollutants as a colorless and water-soluble gas. SO_2 is also emitted by not only natural activities such as volcanic activity and forest fires, but also mostly anthropogenic sources (combustion, smelting, sulfuric acid production, petroleum refining, etc.). In Korea, it is known to be discharged mainly from the fuel combustion process of industrial, heating, transportation, and power generation facilities (Gao et al., 2009). SO_2 stimulates the membrane of the human body, causing respiratory diseases. Furthermore, it reacts with water vapor in the atmosphere, which generates acid rain.

When SO_2 becomes the other sulfur oxides (SO_x) and sulfate ion (SO_4^{2-}), it reacts with other air pollutants such as VOCs to generate small particles. That particle is secondary particulate matters. Therefore, sulfur dioxide causes the secondary contamination as well as primary air pollution (Huang et al., 2014).

Table 2. Characteristic of sulfur dioxide

Characteristic	Contents
State in ambient temperature	Air
Boiling/melting point	-10°C/-75.5°C
Vapor pressure	330 kPa (20°C)
Solubility	8.5 g/100 ml
Specific gravity	2.811 (water=1)
Molecular weight	64.1
Carcinogenesis	IARC: Group 3 ACGIH: A4

Unlike PM_{10}, the air quality standards for SO_2 are regulated as 10 minutes, 1 hour, 3 hours, 24 hours, and yearly average concentration. Although all countries did not regulate total standards, they apply different standards in each country. The standard concentrations of SO_2 in Korea are considered as hourly average value is 0.15 ppm, daily average value is 0.05 ppm, and yearly average level is 0.02 ppm.

Comparing to the SO_2 air quality standards of other countries, the regulation of Korea is middle level in the world similar as China and Hong Kong. Other countries which regulate stronger than Korea are

the UK, Europe, WHO, the USA, and Japan. On the other hands, Unlike the case of PM_{10}, Austria and Canada apply the low regulation of SO_2 level. The reason China had strong regulation about SO_2 unlikely PM_{10} is that SO_2 emissions from industrial complexes in China have been a big problem for air pollution in the world before few decades (Table 3).

Table 3. The standards for sulfur dioxide in atmosphere by countries

	SO_2				
	10 min	1 hour	3 hours	24 hours	Yearly
Korea		0.15 ppm		0.05 ppm	0.02 ppm
USA		0.075 ppm	0.5 ppm		
Japan		0.1 ppm		0.04 ppm	
Canada		900 μg/m^3		300 μg/m^3	60 μg/m^3
Australia		0.2 ppm		0.08 ppm	0.02 ppm
Hong Kong	500 μg/m^3			125 μg/m^3	
China		500 μg/m^3		150 μg/m^3	60 μg/m^3
UK		350 μg/m^3		125 μg/m^3	
EU		350 μg/m^3		125 μg/m^3	
WHO	500 μg/m^3			20 μg/m^3	

1.3 Ulsan city

Ulsan is located in the southeastern part of South Korea, and it is a metropolitan city with a population of more than 1.1 million. On the east coast of Ulsan, there are many industrial complexes, including Mipo National Industrial Area and Onsan National Industrial Area; these areas house petrochemical, nonferrous, automobile, and shipbuilding industries. Next to industrial areas, residential areas are concentrated along the Teahwa river, the biggest river in Ulsan (Figure 4).

Because of the abundance of industrial activity, Ulsan has the highest total productivity per person of all regions in South Korea. However, owing to all this activity, the air in the city is very polluted. In 1986, Ulsan city was selected for the application of special countermeasures against air pollution, and a strict standard of air pollution was enforced.
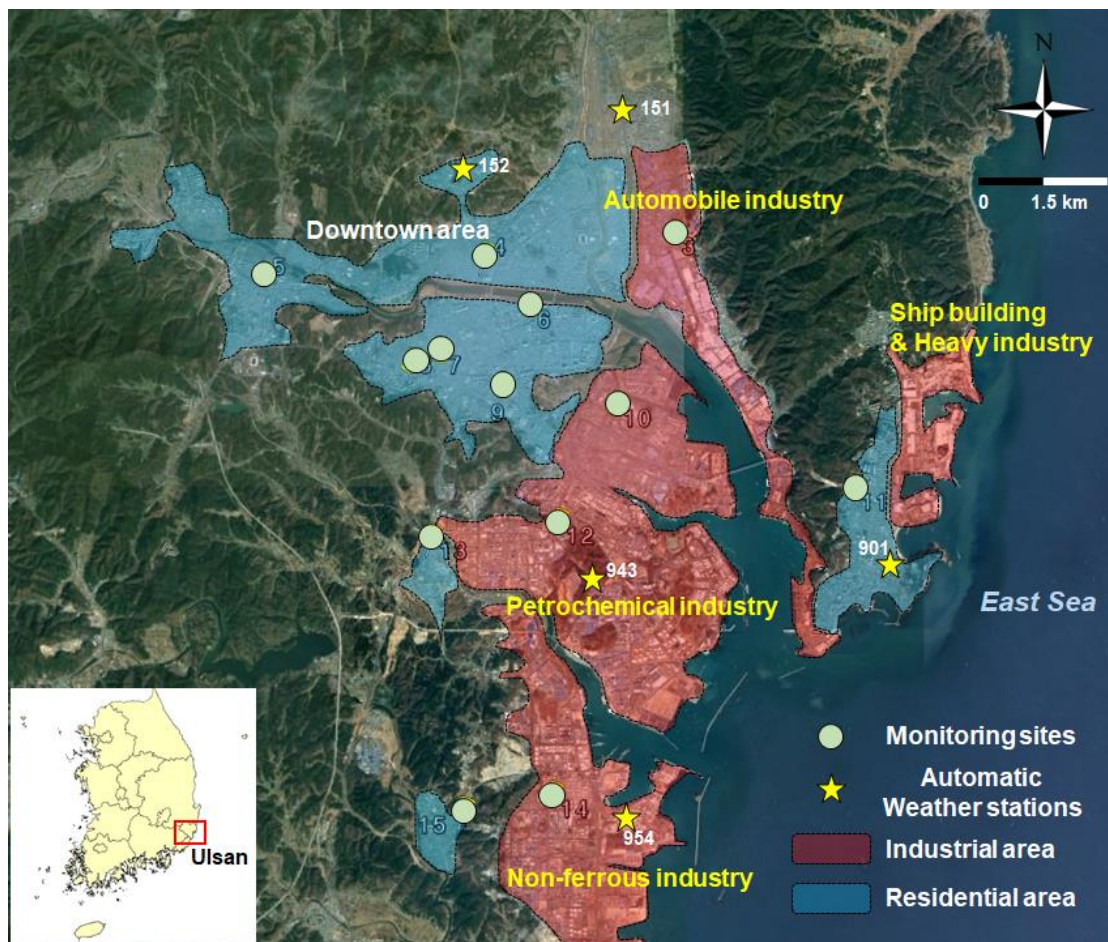
Figure 4. Residential area and industrial area in Ulsan

Compared to other metropolitan cities, the amounts of PM_{10} and SO_2 emissions in Ulsan are the highest. Especially, the SO_2 emissions of the city are considerably higher than those of other cities. The amount of pollutants emitted represents the local sources effect. Given that PM_{10} is affected by LRAT sources, it is difficult to identify the source of pollutants based solely on local emissions. By contrast, SO_2 emission is influenced largely by local sources, so the emission amounts and the sources of pollution are related (Figure 5).

Ulsan was designated as a specific industrial district in 1962, and since then, environmental pollution caused by SO_2 and the damage caused by it to residents' health has been reported. At that time, a large national industrial area (Ulsan, Mipo, Onsan) was established. Despite the efforts of Ulsan city, the annual average concentration of SO_2 has not decreased in recent years and remains at the highest level among the metropolitan cities in Korea. In addition, it is expected that air pollution is being accelerated because the city is planning to continuously expand the urban sprawl and industrial complexes (Lee et al., 2011).
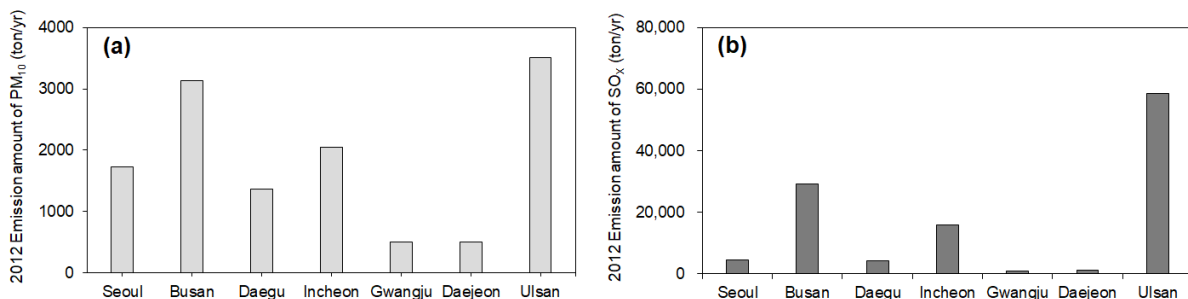
Figure 5. Emission amount of (a) PM_{10} and (b) SO_2 by metropolitan cities in Korea

1.4 Objectives of this study

In this study, the designated study area is Ulsan. The pollution characteristics of PM_{10} and SO_2 are analyzed by using hourly concentration data obtained by monitoring stations in Ulsan. Seasonal and monthly variations of PM_{10} and SO_2 levels are analyzed, and pollution characteristics are analyzed by type of region such as industrial, residential, and roadside area. Correlation analysis of PM_{10} and SO_2 is performed to determine the relationship between pollutants and sources.

In addition, several models are applied to identify the sources. First, the surface wind field is simulated using the CALMET model; then, the wind velocity and wind direction of the monthly and seasonal surface winds are obtained. The emissions of PM_{10} and SO_2 from the stacks are estimated to be dispersed and influenced according to CALPUFF, an air dispersion model. The amount of emission from point sources is determined from the 2012 Clean Air Policy Support System (CAPSS) data. The HYSPLIT model is used to trace the trajectory of air over the large scale and to identify the source of contamination from LRAT by using the hybrid receptor model, PSCF.

Finally, these results are analyzed using statistical methods. Using the conditional bivariate probability function (CBPF), the local sources are identified approximately based on the frequency of wind direction and wind speed when high concentrations of pollutants are found. Many backward trajectories were divided by several groups by performing cluster analysis to identify LRAT sources. Using the Conditional Inference Tree (CIT) and the RandomForest methods, the importance of pollutant variables and the influence of the pollutants are analyzed.

Specific sources of PM_{10} and SO_2 in Ulsan are identified and their influence on residential areas is determined. The purpose of this study was to provide basic information for improving the atmosphere in Ulsan.
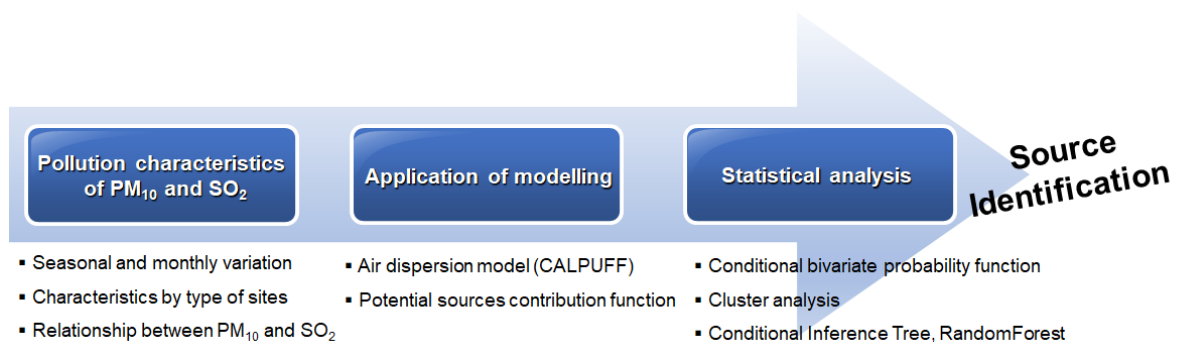
Figure 6. The procedure and objective of this study

II. MATERIALS AND METHODS

2.1 Monitoring stations

The Ulsan Institute of Health and Environment have managed 14 stations of monitoring sites to measure CAPs, such as PM_{10}, SO_2, CO, O_3, and NO_2. The stations provide hourly data of CAPs to people. At each station, a continuous particulate monitor applying a β-Ray absorption method measured PM_{10}, and SO_2 was measured by a pulse UV fluorescence method (Clarke et al., 2014) (Figure 7). For this study, the hourly data of PM_{10} and SO_2 were used during the 1 year, 2012 (January 1-December 31). Monitoring sites are divided a residential area (Nongso, Seongnam, Mugeo, Samsan, Sinjeong, Yaeum, Daesong, Sangnam, Deoksin) and industrial area (Hyomun, Yeocheon, Bugok, and Hwasan), roadside area(Sinjeong-road) (Table 4). The characteristics of downtown areas were the high population density and traffic volume, and industrial areas were composed of automobile industry site, petrochemical industry site, and non-ferrous industry site. In these areas, Figure 8 shows monitoring sites covered downtown sites and each industrial site. This study identified the sources of PM_{10} and SO_2 to research these sites.

Table 4. The information of monitoring stations

Station name	Area type	Longitude	Latitude
Nongso	Residential area	129.35365	35.62541
Hyomun	Industrial area	129.36933	35.56109
Seongnam	Residential area	129.31873	35.55383
Mugeo	Residential area	129.25934	35.55172
Samsan	Residential area	129.33014	35.54414
Sinjeong	Residential area	129.29862	35.53146
Sinjeong-road	Roadside area	129.30056	35.53104
Yaeum	Residential area	129.32465	35.52646
Yeocheon	Industrial area	129.35867	35.51573
Daesong	Residential area	129.41662	35.50357
Bugok	Industrial area	129.33802	35.49652
Sangnam	Residential area	129.31208	35.43441
Hwasan	Industrial area	129.33675	35.43687
Deoksin	Residential area	129.31242	35.43411
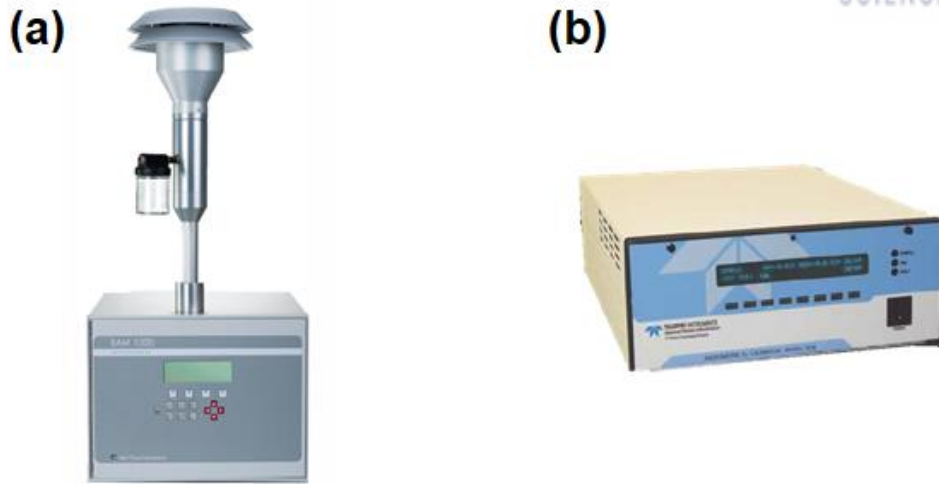
Figure 7. Hourly automatically measuring instruments of (a) PM_{10} and (b) SO_2
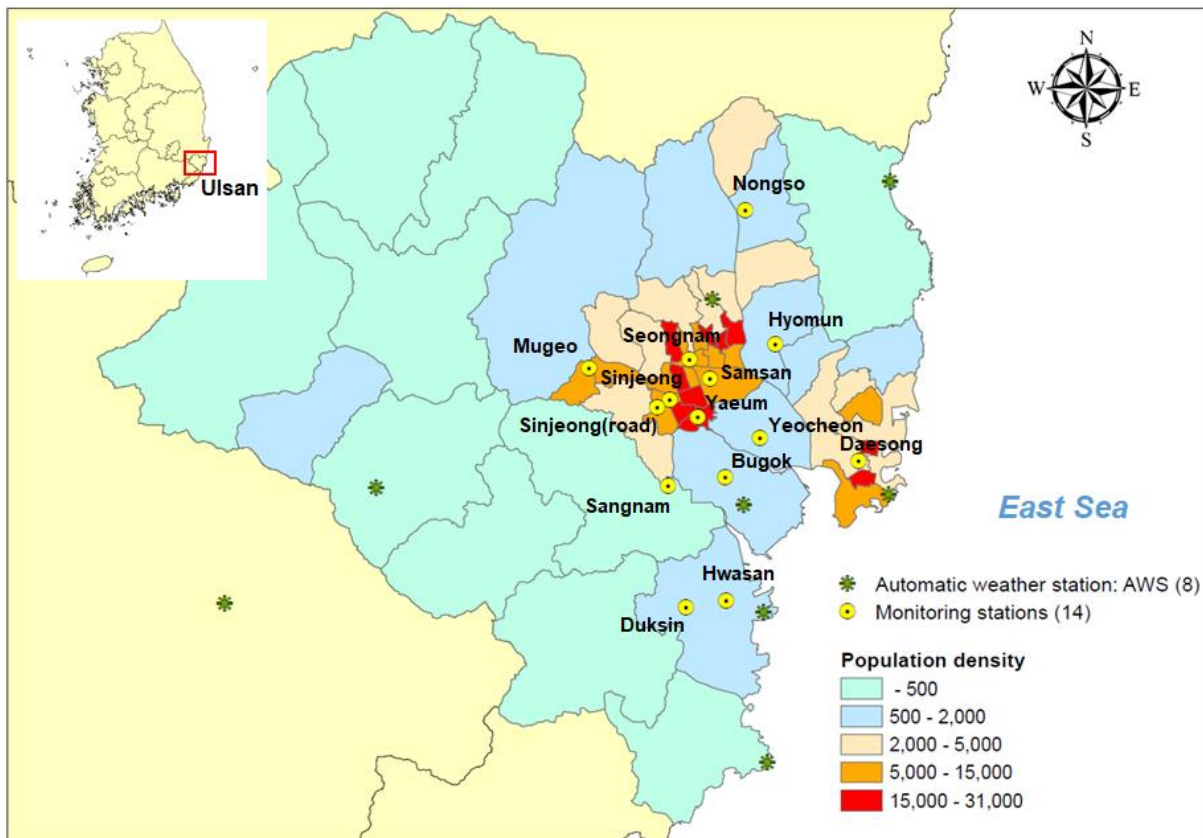
Figure 8. Location of monitoring stations and automatic weather stations

2.2 Meteorological conditions in Ulsan

Eight Automatic Weather Systems (AWS) are operated by the Korea Meteorological Service (KMA) and provide meteorological data. This study need data provided from KMA such as wind speed, wind direction, sea-level pressure, precipitation, humidity, and temperature. Meteorological data were also used hourly data during the 1 year (2012). Seasonal data was distinguished a spring (March 1-May 31), summer (June 1-Augest 31), fall (September1 –November 30), and winter (January 1-February 29, December 1 – December 31, 2012). Among the 8 AWS stations, the 5 stations since the distance between monitoring site and AWS station is considered (Figure 9). For example, the wind data of 152 station is considered when the data of monitoring stations (Mugeo, Seongnam, Samsan, Sinjeong, Sinjeong-road, and Yaeum) was interpreted. However, in CALMET and CALPUFF model, the data of meteorological data of all stations (8 stations) was used.
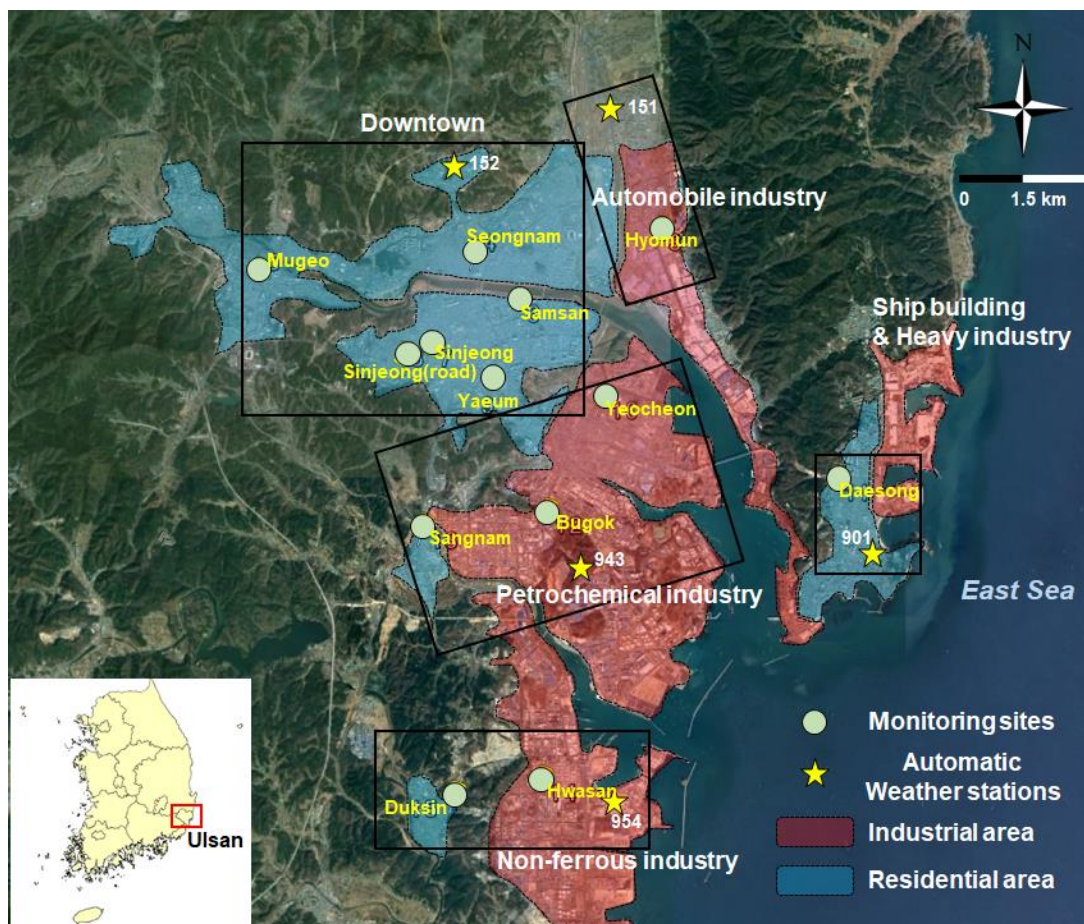
Figure 9. Classifying monitoring station groups as location of AWS

2.3 Conditional bivariate probability function

Conditional bivariate probability function (CBPF) is used in open-air software. The open-air software is written in R-programming language, an open-source programming language that is widely used for data/statistical analysis (W. N. Venables et al., 2018). This software, one of the R packages, and it is used for statistical analysis of air pollution (Carslaw and Ropkins, 2012) in conjunction with meteorological data and various plots. Among these plots, the CBPF plot comprises wind speed, wind direction, and concentration of air pollutants. It calculates data by using the following formula pertaining to conditional probability:

$$CBPF_{\Delta\theta,\Delta u} = \frac{m_{\Delta\theta,\Delta u}|C \geq x}{n_{\Delta\theta,\Delta u}}$$

$m_{\Delta\theta,\Delta u}$ is the number of samples in wind sector $\Delta\theta$ and wind speed Δu within a range of concentration C, and $n_{\Delta\theta,\Delta u}$ is the total number of samples from wind sector $\Delta\theta$ and wind speed Δu (Uria-Tellaetxe and Carslaw, 2014). It can consider the direction of the wind having a concentration of pollutants in a range among the total wind data, and speed of the wind. Information about the pollutants in a specific density range can be used to easily identify the sources of wind by using the CBPF plot. It is easy to identify multiple sources as concentration levels. For example, k-means clustering and bivariate polar plots, which are included in the open-air functions, were used to characterize and understand emission sources (Carslaw and Beevers, 2013). However, the sources were identified based only on wind direction, which does not represent the accurate location of the sources. Moreover, the greater the distance between a monitoring point and a source, the more difficult it becomes to define the specific location of the source. To identify the specific location, wind flow must be predicted using an air dispersion model.

2.4 Clean Air Support System

The Clean Air Support System (CAPSS) based on Air Pollution Emission Inventory provides emission data of eight air pollutants (CO, NO_X, SO_X, TSP, PM_{10}, $PM_{2.5}$, VOC, NH_3) emitted from point, mobile, and area source. CAPSS data in 2012 was provided from National Institute of Environmental Research (NIER) of Korea. 2012 CAPSS data. The emission sources in 2012 are classified by four levels of Source Classification Category (SCC). Four levels consist of upper level categories (SCC1), intermediate-level categories (SCC2), lower-level categories (SCC3), and detail-level categories (SCC4). CAPSS data is separated by not only emission sources but also fuels. There are two levels to be classified by fuels, which are upper-level categories (Fuel1) and lower-level categories (Fuel2) (Figure 10) (Kim et al., 2017; Lee et al., 2011).

In this study, only point source data was used in 2012 CAPSS. The reason is that the point sources only emitting pollutants from the stack directly indicated the effect of industrial complexes. Even area sources emit the pollutants by industrial activities, but it is hard to conclude the effect of industrial complexes completely because they included some non-industrial emissions. Despite the emission amount was underestimated by industrial activities when only point source was used, the effect of location and time variation was indicated well if the relative concentration was considered.
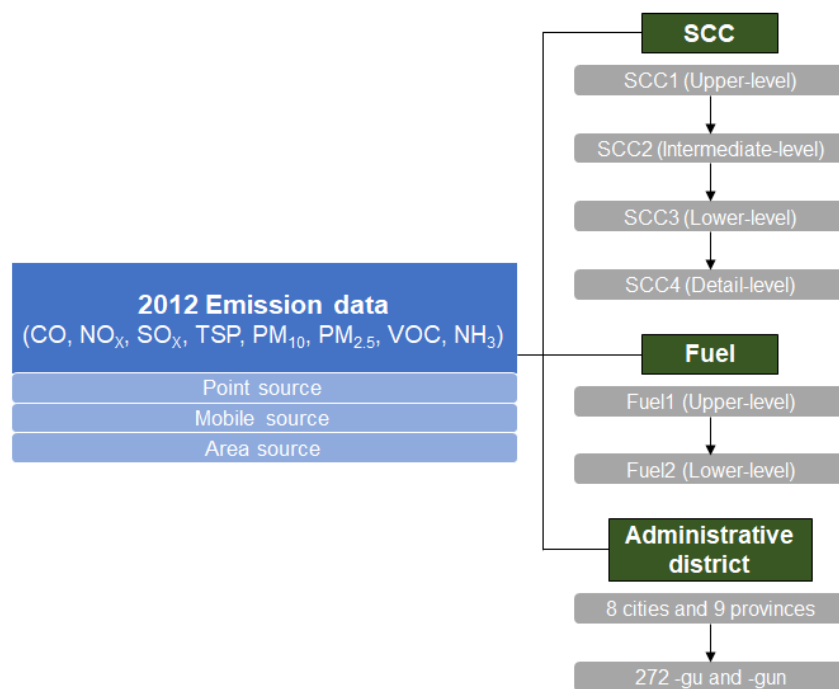
Figure 10. Classification of emission inventory in CAPSS data

2.5 California puff model

To calculate the contribution of emission point sources, we need to predict the flow of air pollutants and their concentration by using an dispersion modeling program such as CALPUFF.

The CALPUFF modeling system is composed of three main parts, namely, the CALMET meteorological model, CALPUFF dispersion model, and CALPOST for processing results files (Scire et al., 2000). CALMET generates a diagnostic three-dimensional meteorological field by considering land cover map, topography, altitude, coastline data, surface meteorological data, and upper air meteorological data. A grid system is generated based on the CALMET field to efficiently calculate the movement of wind and the concentrations of pollutants (Figure 11) (Scire et al., 2000).

CALPUFF is based on a Gaussian puff model, in which a puff moves average wind in a three-dimensional wind field, disperses it by means of turbulence as a Gaussian distribution, and calculates concentrations in a three-dimensional receptor grid (Robert et al., 2005). In comparison to the plume model (i.e., AERMOD), the puff model can consider a variety meteorological conditions for over long term and complex terrain, as well as previous emissions data, when calculating pollutant concentration (Figure 11) (Alan and Robert, 2011).

After simulating air dispersion by using CALPUFF, CALPOST conducts the post procedure to get obtain concentration in the form of a time series. It provides the concentration at each point. These data are drawn as a contour plot by CALPLOT.

In this study, to confirm the flow of wind in a three-dimensional wind field, CALMET was used along with meteorological, terrain, land use, coastline data (Table 5). The results obtained in each season in the Ulsan area are shown. Then, to identify the patters of pollutant dispersal from point sources, 2012 CAPSS data were used as the emission data for CALPUFF modeling. The number of point sources was set to 124 (Figure 12). In addition, the information input into CALMET and CALPUFF is summarized in Table 6.

Because the industrial activity is one of the main PM_{10} and SO_2 sources, CALPUFF results pertaining to the dispersion of CAPs could predict the influence of residential areas. To identify the main sources of PM_{10} and SO_2, the dispersion patterns of pollutants and their influence are important.
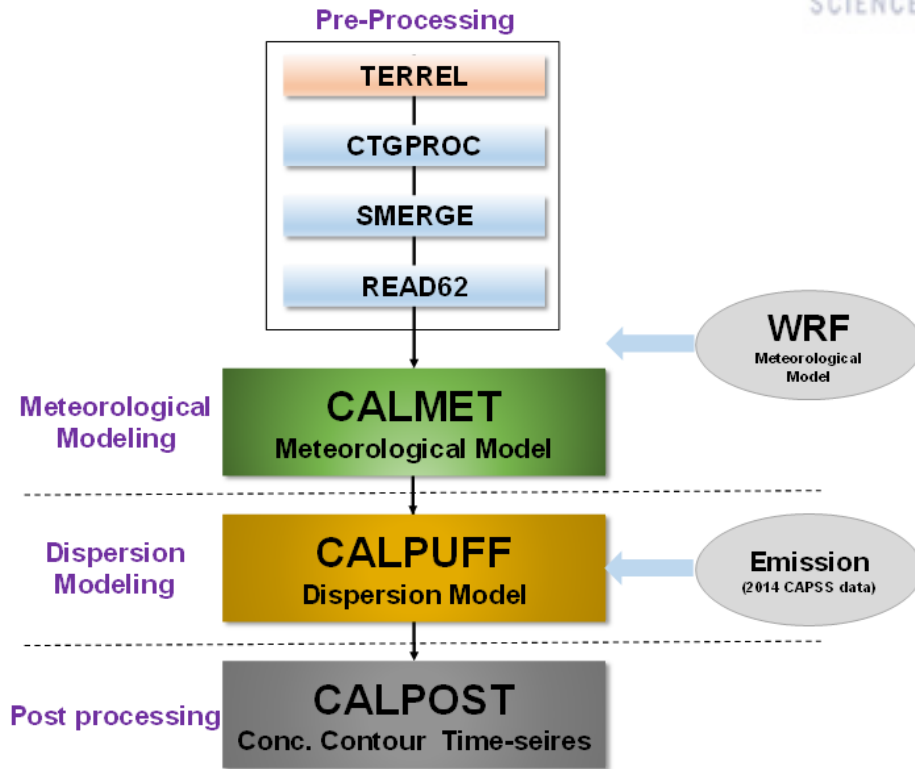
Figure 11. Diagram of CALMET, CALPUFF and CALPOST model
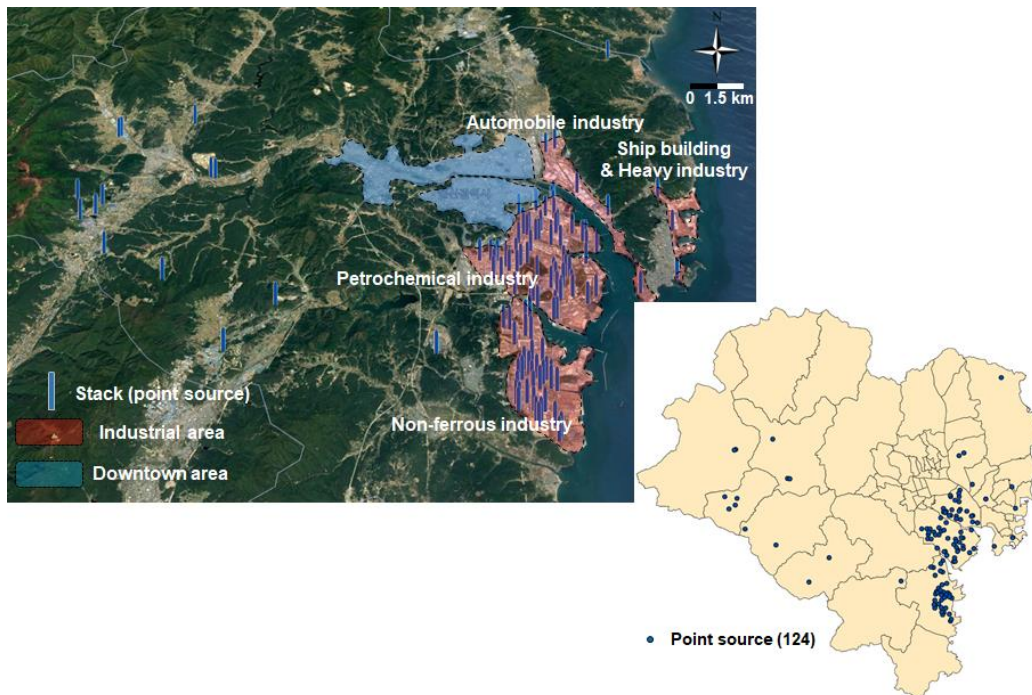
Figure 12. Location of point sources in Ulsan

Table 5. Topography and meteorological data of CALPUFF in study area

Data	Contents
Terrain data	ASTGTM 2_N35E139
Land use data	(GLAZAS) USGS Global for Eurasia Asia
Coastline data	Gshhs_f.b (NOAA)
Surface Met data	152, 854, 901, 905, 924, 943, 949, 954 station (AWS)
Upper Met data	47138 station (NOAA/ESRL Radiosonde Database)

Table 6. Input data of CALPUFF model

Data	Contents
Grid origin	X: 495 km E, Y: 3905 km N
Domain size	50 × 50 km (Grid spacing: 1 × 1 km)
Cells	NX(50), NY(50), NZ(12)
Projection	Universal Transverse Mercator (UTM)
Vertical layer	12 layers (20, 50, 80, 160, 300, 600, 1000, 1500, 2200, 3000, 4000, 5000 m)
Time zone	UTC+0900
Modeling period	2012.01.01 – 2013.01.01

2.6 Backward trajectory analysis

Recently, many researchers have used backward trajectory to analyze the effect of LRAT by employing the HYSPLIT model developed by NOAA. Backward trajectory analysis is performed mainly to analyze the phenomenon of air mass movement by analyzing upper-layer weather information. Backward trajectory analysis can be used to check changes in wind speed along the trajectory and direction of pollutants (Lin et al., 2014; Sait et al., 2013).

In this study, backward trajectory analysis was performed to identify the LRAT effect of PM_{10}. LRAT occurs mainly in the upper air, not on the surface. It occurs below the mixing height layer (Daria et al., 2017), which is generally considered to be 500 m above the ground (Lee et al., 2016). To consider the effects of China and Japan, which are near Korea, the period of backward trajectory set to three days. Therefore, the backward trajectory of three days was analyzed at 0, 6, 18, and 24 h every day. The backward trajectory of 2012 (January 2012–January 2013) was analyzed monthly and seasonally (Table 7). The backward trajectories were interpreted by means of time series analysis and cluster analysis. Cluster spatial variance (SPVAR), which is the square of the distance between the endpoints, was calculated for each backward trajectory to select the number of clusters. The number of clusters was determined based on the variation of the total spatial variance (TSV), which was computed as the sum of SPVAR values, when the amount of change in TSV increased or decreased (Song et al., 2017). In this study, five clusters were set up (Figure 13).

To determine why the concentration distribution of particulate matters in Ulsan showed seasonal variation, we considered that the level of PM_{10} by was influenced by external LRAT sources. To identify the potential sources from a long distance, the hybrid receptor model and the potential contribution source function (PSCF) were used. The PSCF model is a probability map that the trajectory passing through a specific lattice point reaches a receptor point at which the pollutant concentration is higher than the set criterion for PM_{10} level. In this study, PSCF was analyzed to interpret the backward trajectory and cluster analysis (Han et al., 2004; Choi et al., 2011). PSCF value was calculated using the following equation. m_{ij} denotes the number of trajectories passing through the ij grid cell that have higher values than the pollution criterion level the in the ij grid cell, and n_{ij} is the number of trajectories passing through the ij grid cell (Jeong et al., 2017). Weight value is considered in the PSCF calculation. The higher the number of trajectories passing through the cell, the higher is the weight. The weight value is listed in Table 8 (Stojic and Stojic, 2017).

$$PSCF_{ij} = {m_{ij}}/{n_{ij}}$$

Table 7. Input data of HYSPLIT model

Data	Contents
Location	Sinjeong monitoring station
Coordinate	35.5404 N, 129.3147 E
Study period	2012.01.01 – 2013.01.01
Trajectory period	72 hours
Height	500 m a.g.l
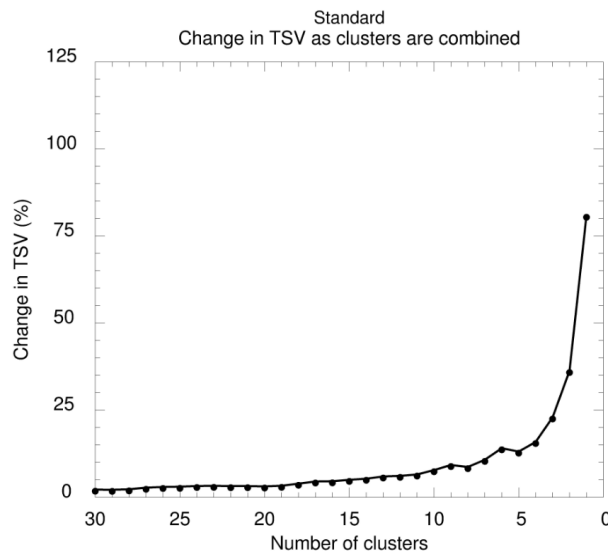
Figure 13. Changes in TSV according to the number of clusters

Table 8. Input data of PSCF model

Data	Contents
Model	TrajStat (developed by Yaqiang Wang)
Domain	$50º \times 40º$ (cell size: $0.5º \times 0.5º$)
Pollution criterion	Top of 25% level, top of 75% level, and the average level
Weight	$W(nij) = \begin{cases} 1, & n \geq 2\,av \\ 0.75, & 2\,av \geq n \geq av \\ 0.5, & av \geq n \geq \dfrac{av}{2} \\ 0.2, & \dfrac{av}{2} \geq n \end{cases}$

2.7 Conditional Inference Tree

Decision tree learning, a machine learning method, is commonly used in data mining (Torgyn et al., 2017). The goal of the method is to create a model that predicts the value of a target variable based on several input variables. In a tree structure, each internal node corresponds to one input variable, and the branches to child nodes correspond to the possible values of the input variable. A leaf node corresponds to a target variable value when each input variable has a value corresponding to a path from a root node to a leaf node (Leo et al., 1984).

The objectives of decision tree are segmentation, classification, prediction, data reduction and variable screening, and identification of interaction effect. A decision tree can indicate the contents of these parts (Hothron et al., 2006). There are many types of decision tree algorithms, such as ID3, C5.0, classification and regression tree (CART), chi-squared automatic interaction detector (CHAID), multivariate adaptive regression splines (MARS), and conditional inference tree (CIT). The algorithms used for statistical analysis are CART, CHAID, MARS, and CIT (Fatin et al., 2017). Among them, CIT overcomes the problem of overfitting. CIT is automatically p-tested, and it statistically analyzes the significance of predictive variables and creates nodes accordingly. Therefore, CIT presents a lower risk of overfitting. In this study, CIT analysis was performed using the "party" package in the R program (Hothorn et al., 2017).

The random forest method is used to create several decision trees by voting in order to determine the result by majority. In a random forest, the bootstrap method is used to form a forest. It is a method of learning by inputting the result of a sample as a tree, as opposed to using all data (Strobl et al., 2008). This results in randomness because each tree is constructed from different data. When dividing the partition, it gives variable randomness. In other words, it selects the best variables among a few selected variables instead of all variables (Breiman, 2001). This approach is called ensemble learning. Random forest is one of the most popular and frequently used algorithms. Because unsampled data is available as test data, the entire data can be used for learning.

III. Results and discussion

3.1 Monitoring results

The monthly average concentrations of PM_{10} were the highest in April and May, and the lowest in August, September, and December (Figure 14). The PM_{10} level increased from January to May, indicating the most polluted season in terms of PM_{10} level was spring. In summer, PM_{10} level tended to decrease, except in July. However, the amount of PM_{10} emission in Ulsan showed an opposite pattern (Figure 16 (a)). The amount of emission during spring was lower than that during summer. This indicated that the local emission impact was lower than that of other sources, such as LRAT or meteorological factors during spring. The average concentration in July was similar to that in the spring, and the standard deviation was the highest. This finding indicates the existence of large differences among the 14 monitoring stations. This phenomenon was expected to be influenced by local sources in July. The concentration increased slightly in the fall. The variation in daily PM_{10} concentration was the highest in spring and the lowest in summer. This indicated the occurrence of a large number of PM_{10} events in April and May. Moreover, there were few events during summer.

The monthly average concentrations of SO_2 showed a tendency opposite to that of PM_{10} (Figure 15). The highest SO_2 level was observed in July and the lowest in March. During April to July, the SO_2 concentration and its standard deviation increased. Because the amount of SO_2 emitted remained constant until August (Figure 16 (b)), the phenomenon of sharp increase in SO_2 was expected to be influenced by another factor such as wind pattern or an external source. After July, the monthly SO_2 concentration decreased sharply, and it remained constant. There were no large variations in the monthly SO_2 level during 2012, except from April to July. The highest daily SO_2 concentration was observed on a day in January, and large variations in SO_2 concentration were observed from April to July.

The PM_{10} concentration in spring showed the highest median value among all seasons (Figure 17 (a)). To derive the statistical difference between seasons, the Mann–Whitney rank sum test was conducted. The result of the rank sum test showed that the PM_{10} concentration in spring was statistically higher than those in the other seasons ($P \leq 0.01$). Among the other seasons, the differences were not statistically significant (summer-fall: $P = 0.918$, summer-winter: $P = 0.997$, fall-winter: $P = 0.866$).

The seasonal SO_2 concentration showed a different pattern compared to that of PM_{10} (Figure 17 (b)). The SO_2 level in summer was the highest, but there was no significant difference between spring and summer according to the rank sum test ($P = 0.059$). A comparison of SO_2 levels among summer, fall,

and winter indicated that the SO_2 level in summer was higher than those in fall and winter ($P \leq 0.01$). The SO_2 level in spring was only higher than that in fall ($P \leq 0.01$) and not statistically significant different from the level in winter ($P = 0.077$). There was no statistically significant difference between fall and winter ($P = 0.214$) as well.
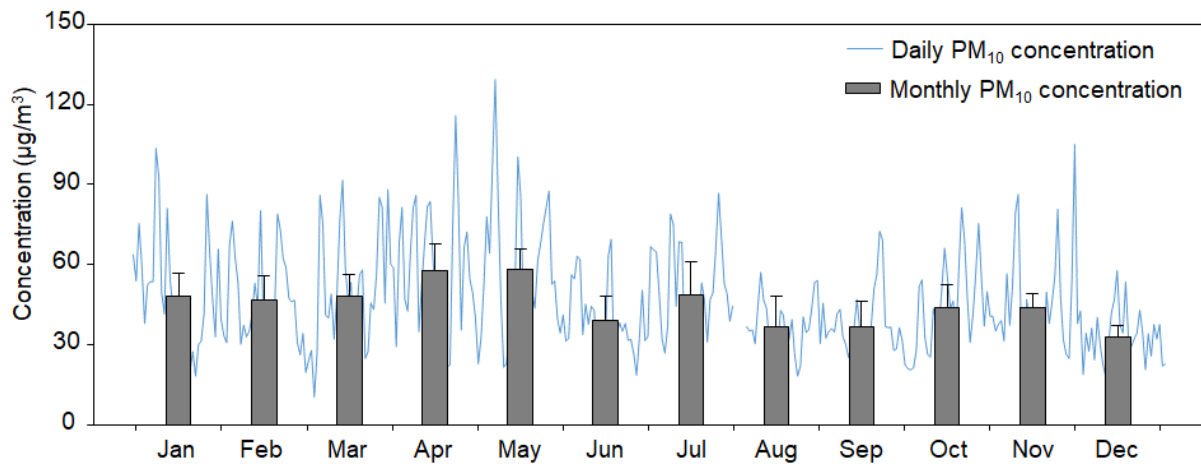
Figure 14. Daily and Monthly variation of PM_{10} concentration in Ulsan
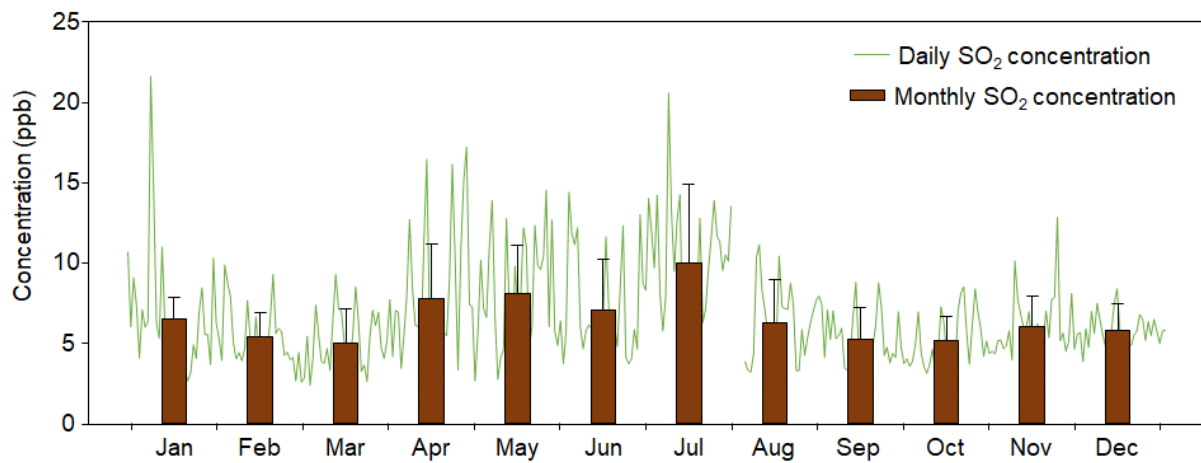
Figure 15. Daily and Monthly variation of SO_2 concentration in Ulsan
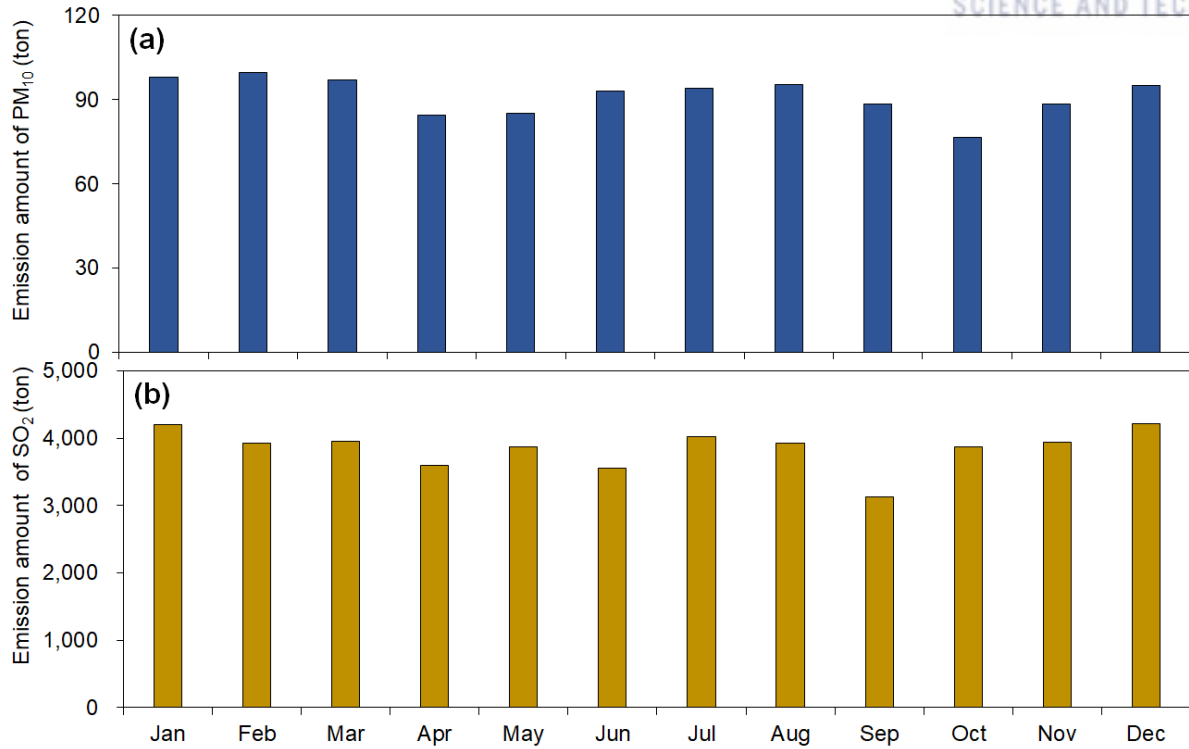
Figure 16. Monthly emission amount of (a) PM_{10} and (b) SO_2 from point sources in Ulsan
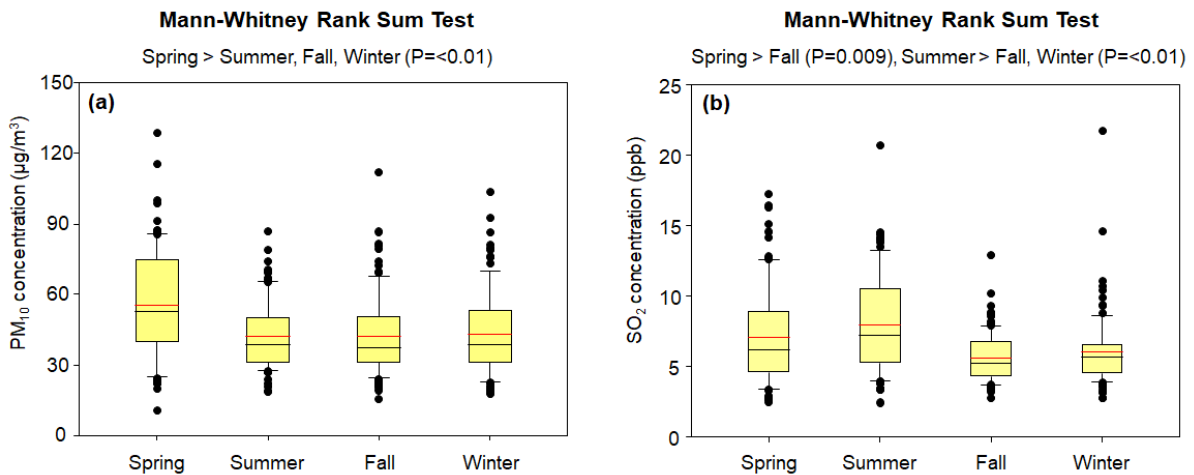
Figure 17. The seasonal concentration and statistical analysis of (a) PM_{10} and (b) SO_2

In Ulsan, the industrial areas were the most polluted by PM_{10} compared to the residential areas and the roadside areas (Figure 16). The monthly variation of PM_{10} was similar in the three areas, indicating an increasing pattern during spring and decreasing pattern during summer and fall, except July. The difference was that the PM_{10} level in the industrial areas decreased in October but that at the other sites

tended to decrease from November. Overall, the monthly variation was the least in the roadside areas. Specifically, the two other areas showed a rapid increase in PM_{10} concentration in July but that in the roadside areas remained constant.

Likewise, the SO_2 concentration showed a similar monthly variation in all three regions, but the difference between industrial areas and the other two areas was larger than that in the case of PM_{10} (Figure 18). Especially, in summer, the SO_2 concentration in the industrial areas increased considerably but that in the roadside areas remained constant. In addition, after September, SO_2 concentrations in industrial areas decreased steadily but those in the residential areas increased slightly owing to residential heating during winter (Figure 19).

The results of the rank sum test for annual concentration showed that the PM_{10} concentration in the industrial areas was statistically higher than those in the other two areas ($P \leq 0.01$) (Figure 20 (a)). The annual SO_2 concentration in the three regions was statistically higher than that of PM_{10}, and the concentration in residential areas was statistically higher than that in the roadside areas (Figure 20 (b)).
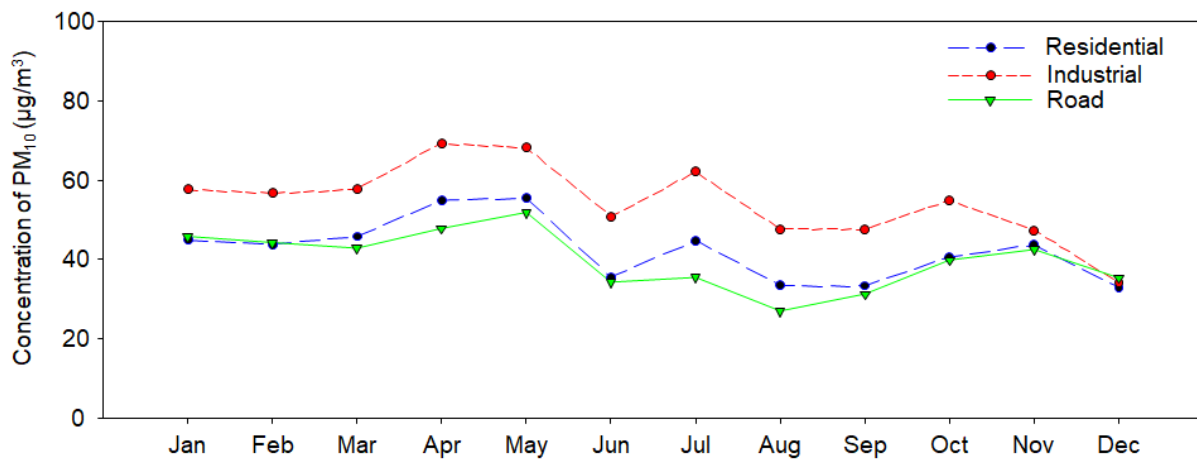
Figure 18. The monthly variation of PM_{10} levels by type of sites
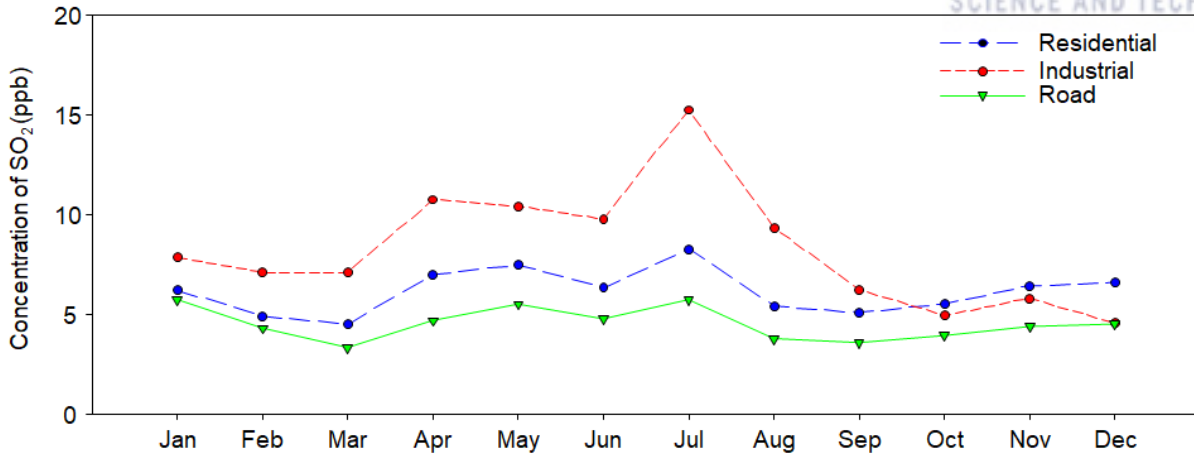
Figure 19. The monthly variation of SO_2 levels by type of sites
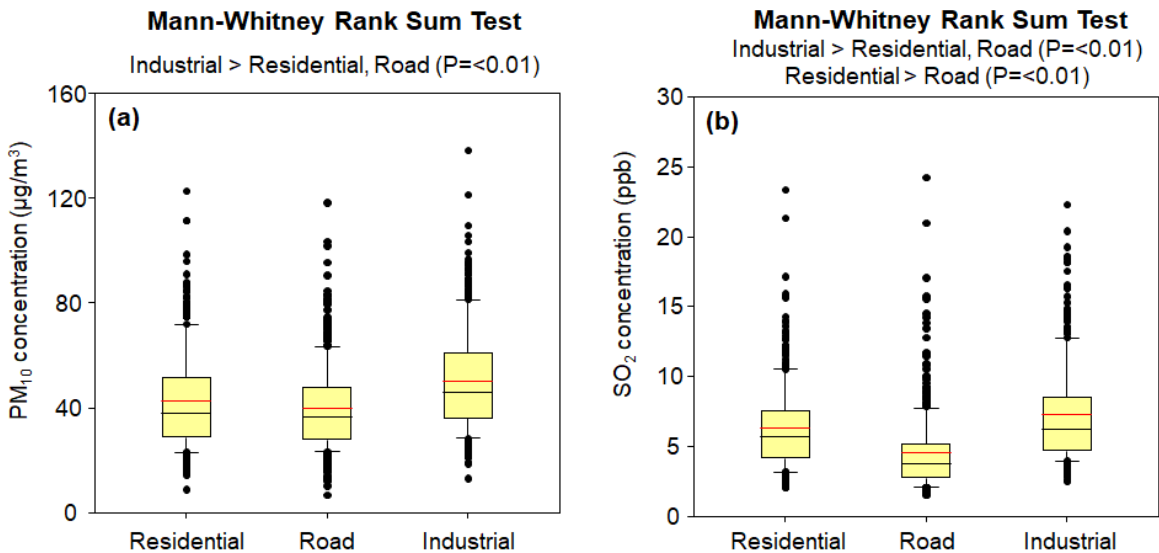
Figure 20. Annual concentration of (a) PM_{10} and (b) SO_2 by three types of area

A statistical analysis of the regional concentrations in each season show that the PM_{10} level in spring was the same as the annual concentration pattern, and the concentration in summer was statistically higher in the residential areas than that in the roadside areas ($P \leq 0.01$) (Figure 21 (a)). In addition, the PM_{10} concentration in spring in the three areas was broader than that in the other seasons, and the differences in PM_{10} concentration among three areas was the largest in summer and the smallest in winter (Figure 21 (b), (c), (d)). The SO_2 concentrations in spring and summer had a wider range than the SO_2 level in fall and winter (Figure 22). In spring and summer, the SO_2 concentration was higher

by a statistically significant margin in the order of industrial, residential and roadside areas ($P \leq 0.01$) (Figure 22 (a), (b)). By contrast, there was no statistically significant difference between the residential and the industrial areas in fall and winter (fall: $P = 0.284$, winter: $P = 0.436$) (Figure 22 (c), (d)).
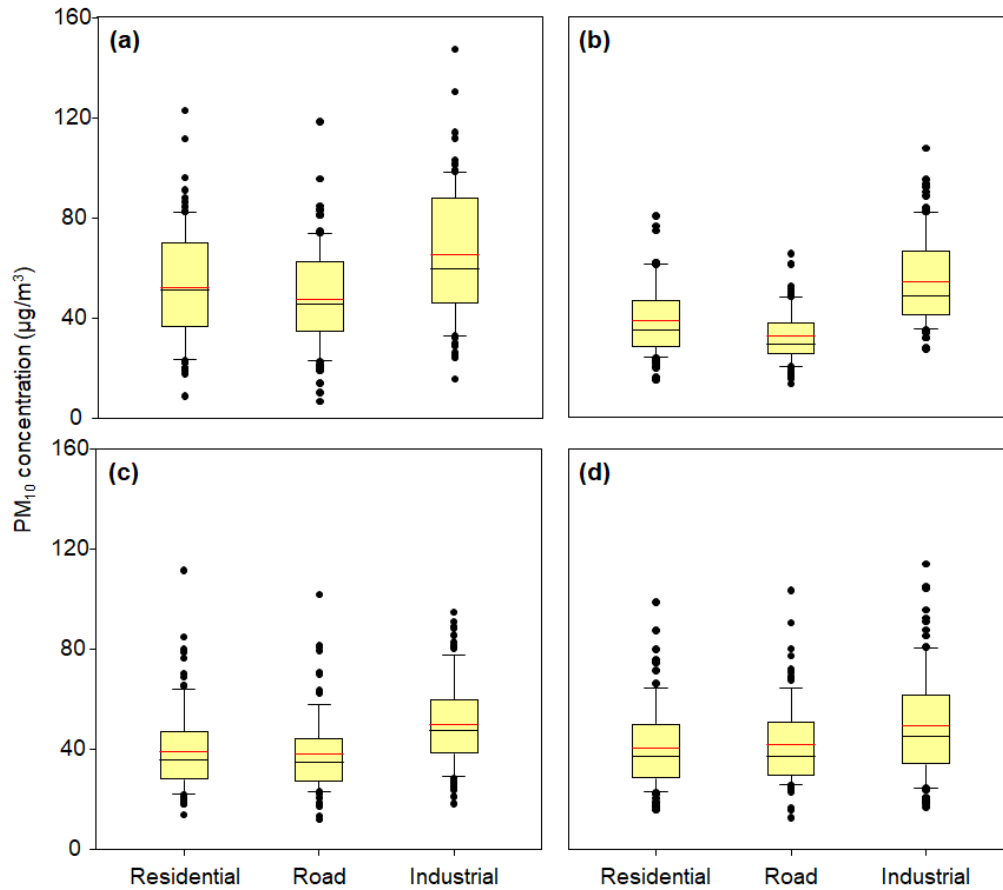
Figure 21. The seasonal concentration of PM_{10} in (a) spring, (b) summer, (c) fall, and (d) winter by areas
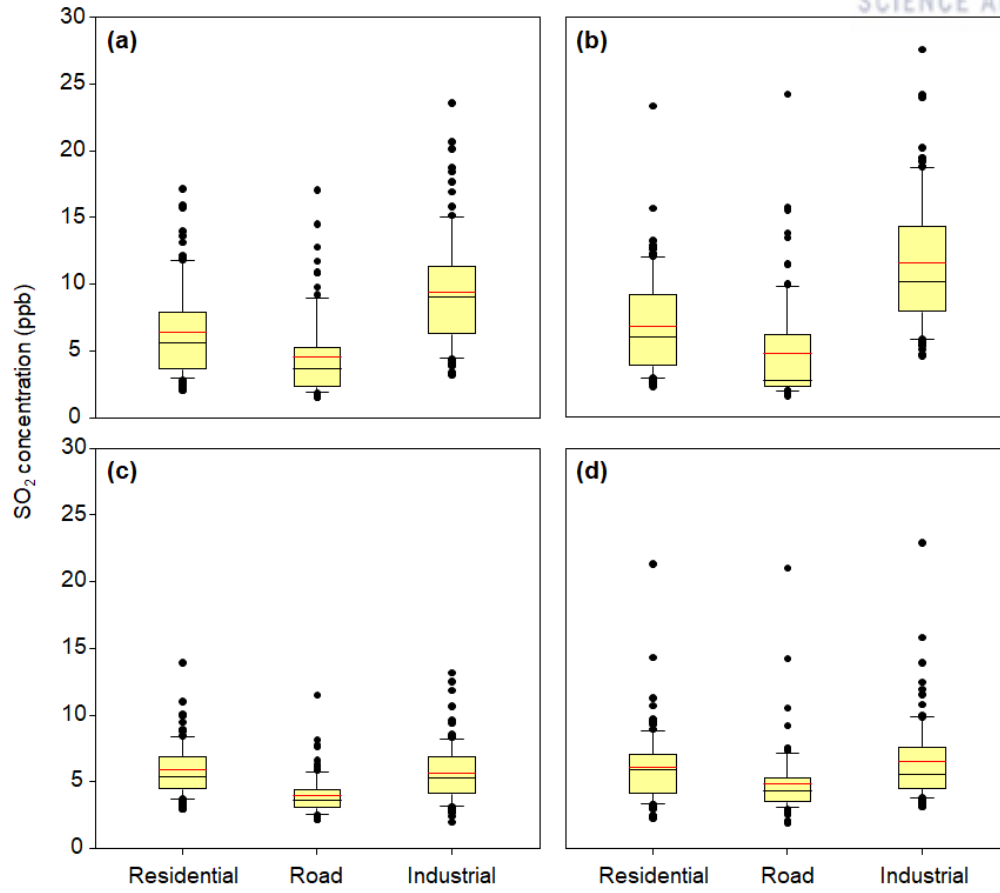
Figure 22. The seasonal concentration of SO_2 in (a) spring, (b) summer, (c) fall, and (d) winter by areas

3.2 Local source identification

3.2.1 Determining representative sites to identify the soures

To identify the sources of PM_{10} and SO_2, representative sites of residential areas should be selected because the application of statistical approaches and models, as well as comparison with monitoring results, are conducted at specific locations. Furthermore, because the goal of this study is to characterize air pollution as experienced by the residents of Ulsan, appropriate sites from the residential, roadside, and industrial areas were selected. The representative residential site was selected considering population and population density. Among the residential areas, including CAPs monitoring site, Yaeum station had the highest population density (Table 9). In the selection of the representative industrial site, we considered amount of PM_{10} and SO_2 emissions from point sources located in a district within the monitoring site. Therefore, Yeochoen station, which was located near the largest point emission sources, was selected as the representative industrial site (Table 10). The roadside site including a CAPs monitoring station was only Sinjeong roadside, which was selected as the representative roadside area.

Table 9. Population information by residential monitoring sites

Station name	District	Population (person)	Rank of population	Population density (person/km^2)	Rank of population density
Nongso	Nongso1dong	29,073	4	1930.5	7
Seongnam	Jungangdong	14,889	8	8758.2	4
Mugeo	Mugeodong	38,134	2	11806.2	2
Samsan	Samsandong	50,954	1	9932.5	3
Sinjeong	Sinjeong2dong	22,723	6	8115.4	5
Yaeum	Daehyundong	31,574	3	27455.7	1
Daesong	Daesongdong	15,591	7	2809.2	6
Sangnam	Chyunryangmyun	14,214	9	239.9	9
Deoksin	Onsaneup	24,720	5	646.1	8

Table 10. Information about emission amount of PM_{10} and SO_2 by industrial monitoring sites

Station name	District	Emission amount of PM_{10} (kg/year)	Emission amount of SO_2 (kg/year)
Hyomun	Hyomundong	18	19
Yeocheon	Yeocheondong	72,672	18,819,092
Bugok	Bugokdong	68,163	1,187,200
Hwasan	Onsaneup	4,307	16,130,473

3.2.2 Relationship between PM_{10} and SO_2 hourly concentration

Because SO_2 has a shorter life-time (12–48 h) in the troposphere than other CAPs materials, the effect of LRT on it was the weakest (Chin et al., 1996; Lin et al., 2005; Manahan, 2009). Especially, Ulsan, which is farther from China than the western part of South Korea, is less affected by China. Hence, the fuel burned in industrial, heating, transport, and power generation facilities in the region is the main source of SO_2 in Ulsan. The correlation between PM_{10} and SO_2 indicated the influence of fuel combustion on the PM_{10} generated from various sources.

First, in case of the residential area, the R^2 value was the lowest in autumn and the highest in winter (Figure 23). This was expected to lead to an increase in the influence of the fuel combustion process in winter, which was indicated as an increase in residential heating. There was the highest slope value in summer. It was interpreted that the SO_2 concentration increased compared to that of PM_{10}. However, the relationship between PM_{10} and SO2 was relatively weak, which indicated that the sources of the two pollutants were different. By the time, the ratio of SO_2 concentration increased at noon in all seasons, except winter. This indicated that the SO_2 source was affected during noon in the residential areas, unlike the PM_{10} source.

The relationship between PM_{10} and SO_2 in Yeocheon, which represented an industrial area, was relatively in spring and winter, as in the case of Yaeum, which was predicted to occur based on increased use of fuel for domestic heating (Figure 24). In autumn, the R^2 value was very small. This means the sources of PM_{10} and SO_2 were different. By the time, the concentration of PM_{10} and SO_2 did not show any specific trends with time.

Lastly, the result of the regression analysis for the roadside area showed an average R^2 value higher than those of the other two areas (Figure 25). It was expected that the effect of PM_{10} and SO_2 on the roadside areas were due to automobile fuel combustion. In winter, the roadside areas showed the highest R^2 value owing to residential heating. In this season, the concentrations of PM_{10} and SO_2 increased the ratio of SO_2 during the daytime, as in the case of the residential areas. This means that the sources of SO_2 affected the pollution levels in the residential and the roadside areas during the daytime.

In summary, the correlation between SO_2 and PM_{10} levels was not significantly in Ulsan. This means that the sources of SO_2 and PM_{10} were different, but the tendency of R^2 to increase in winter indicated that both PM_{10} and SO_2 levels were affected by domestic heating. SO_2 concentration in the residential and the roadside areas tended to increase during the daytime, unlike PM_{10}.
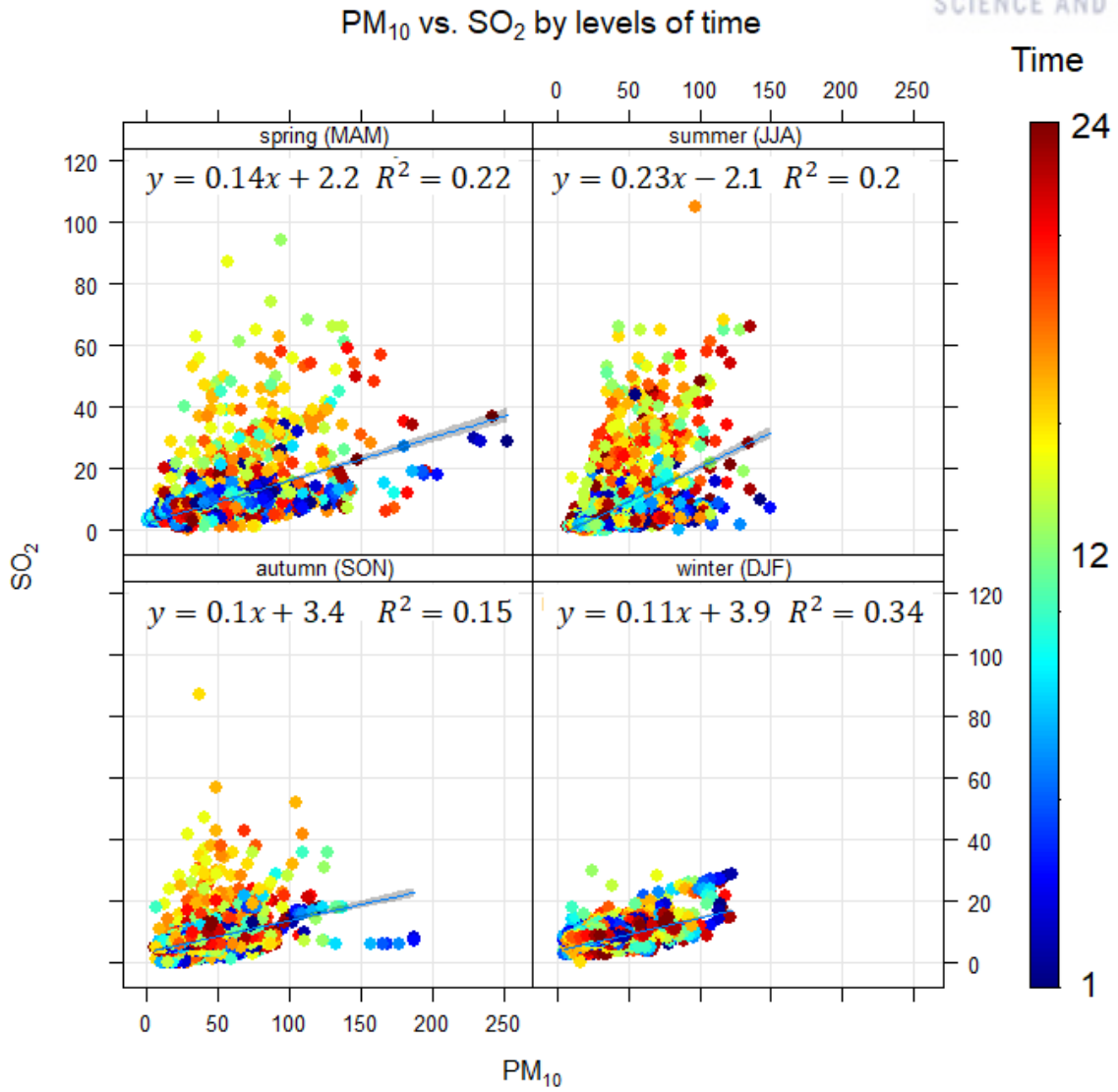
Figure 23. The scatter plot and regression analysis of PM_{10} and SO_2 by level of time in Yaeum
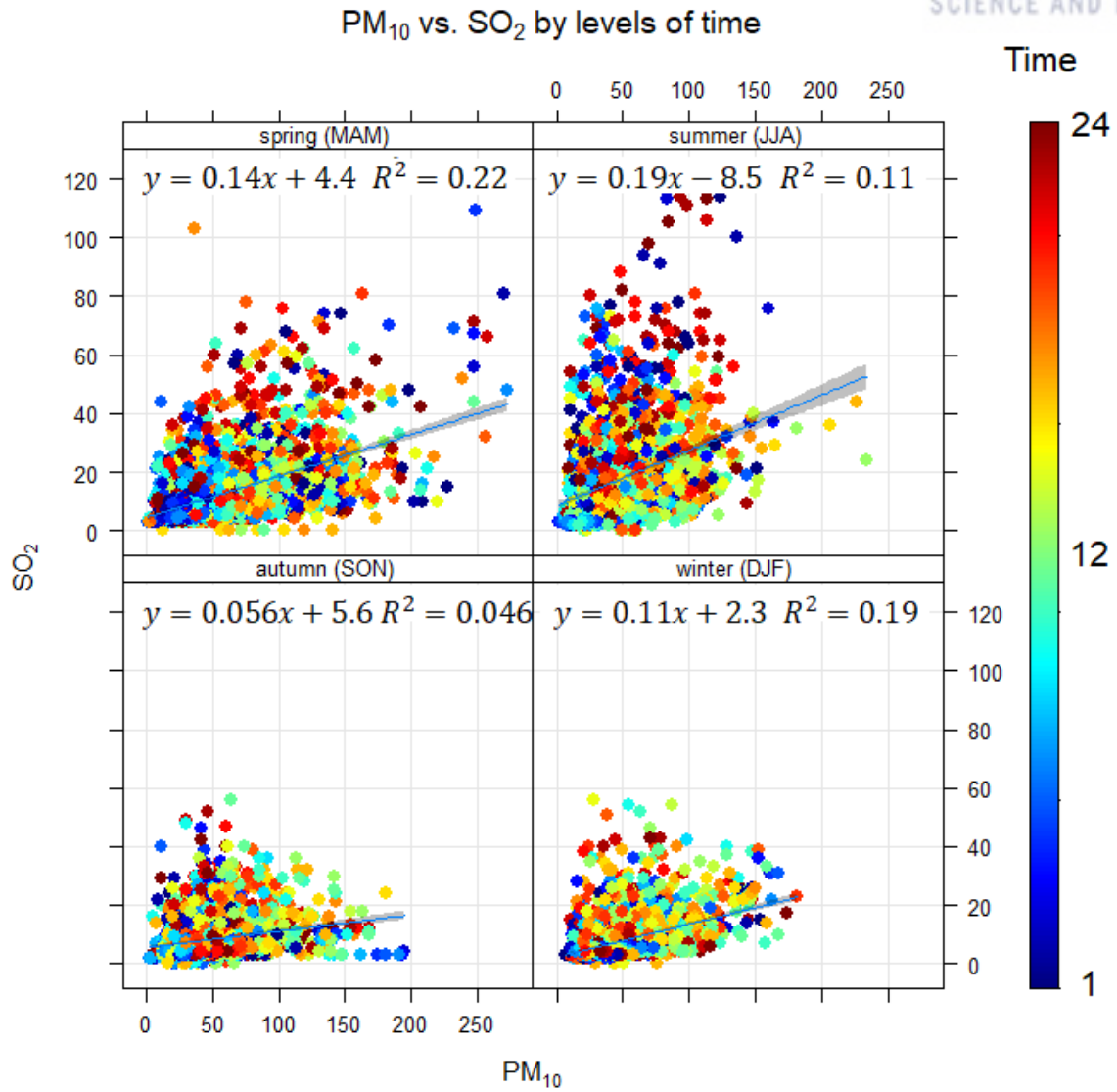
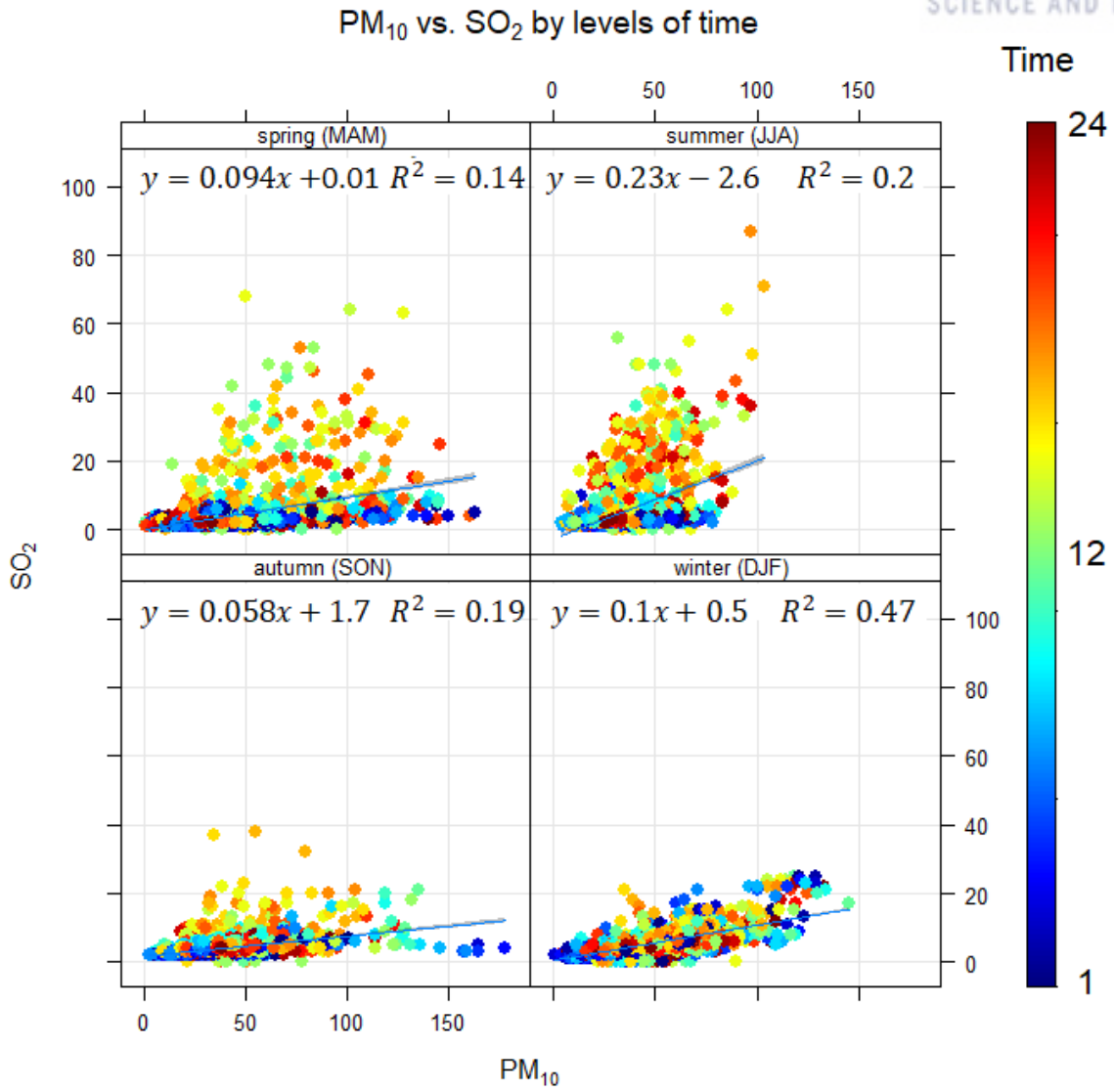Figure 24. The scatter plot and regression analysis of PM_{10} and SO_2 by level of time in Yeocheon

Figure 25. The scatter plot and regression analysis of PM_{10} and SO_2 by level of time in Sinjeong-road

3.2.3 CBPF result of PM_{10} and SO_2

The CBPF plot shows the sources of high concentrations of air pollutants along specific wind directions and speed as conditional probabilities (Carslaw and Beevers, 2013). The plot indicates that it is more appropriate to identify the influence of the local sources that have a periodic effect than that of occasional high-concentration events such as yellow dust (Iratxe and David, 2014). In this study, the approximate locations of the local sources were determined using the CBPF plot with the wind information and the concentrations of PM_{10} and SO_2.

The high concentration PM_{10} in the top 15% results obtained in spring was influenced by the surroundings when the wind speed was weak. The high concentration of particulate matter observed was ascribed to the influence of traffic in residential areas and atmospheric congestion. In the case of Yeocheon, in spring, the PM_{10} concentration of the top 5–15% results were affected in the southwest, and the PM_{10} concentration in the top 5% of the results was affected by winds from the east. It was interpreted that the PM_{10} level was influenced by the winds blowing from petrochemical complexes located around the monitoring site and by winds from the nonferrous industrial complexes located southward. High concentrations of PM_{10} in the roadside areas during spring were considered to influenced by vehicle emissions on the road. In summer, it seems that the PM_{10} level at Yaeum was affected by the industrial complex in the south and the commercial area in the west. The high level of PM_{10} at Yeocheon was affected by the surrounding petrochemical complexes and the nonferrous industrial complexes in south, as in the case of spring. The PM_{10} in the roadside areas had a large influence on the surrounding roads, as in the spring. The high concentration of PM_{10} in residential areas in the fall was influenced by residential and commercial areas in the south-west direction, while the top 5% concentration results were influenced by nearby roads. Local sources of high PM_{10} concentrations in industrial areas were surrounded by petrochemical complexes, and roadside areas were influenced by emission from vehicles in the surrounding. In addition, the top 5% concentration results of the roadside areas were affected by relatively distant sources when the speed of the wind from the north was high. In winter, all three areas were similar to case of fall, and the top of 5–15% results of PM_{10} level in the roadside areas were strongly influenced by winds from the south (Figure 26).
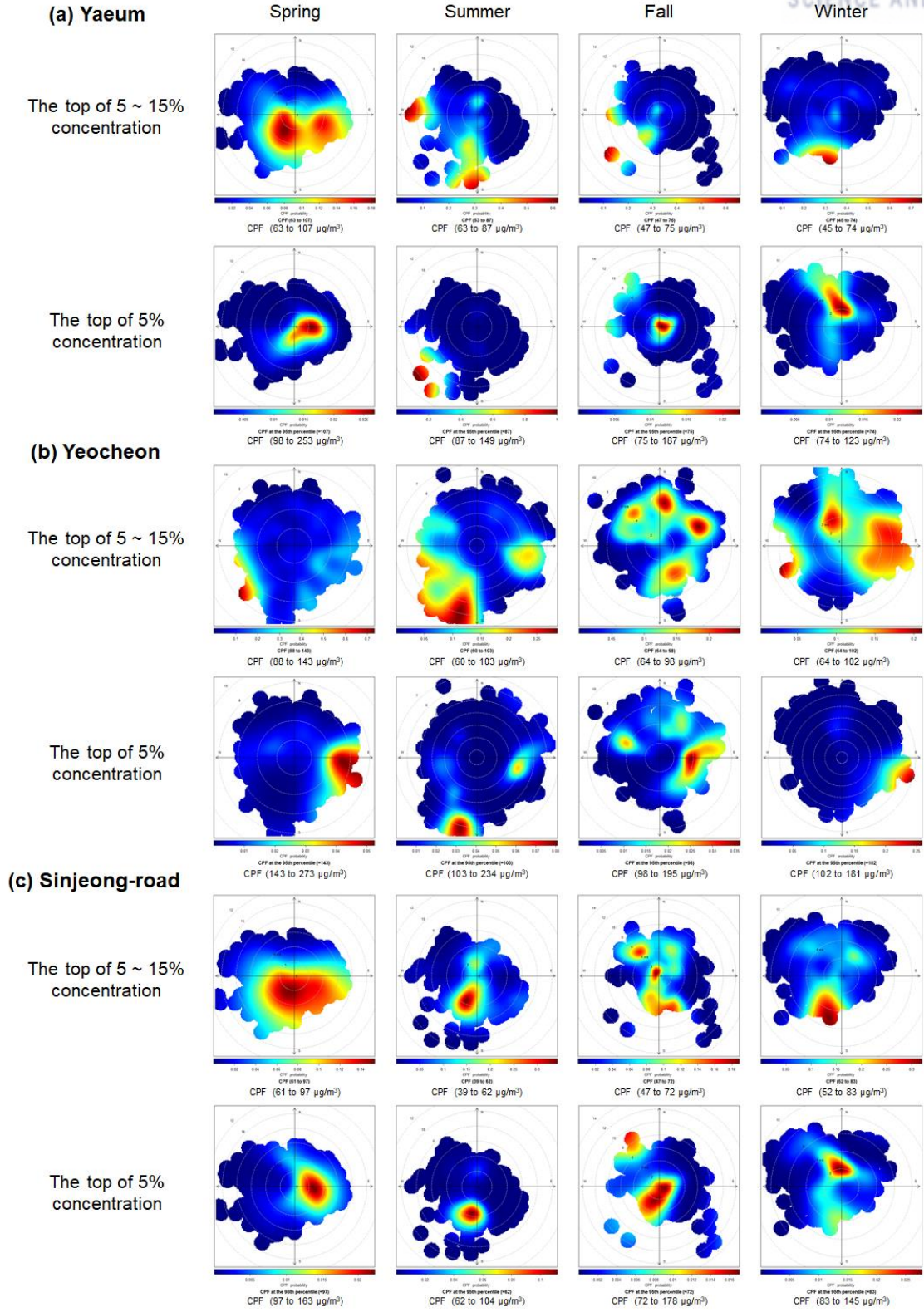
Figure 26. CBPF plot indicating top of 5~15% and 5% concentration of PM_{10} in the three sites

The CBPF plot of high concentration of SO_2 showed a different pattern from that of PM_{10}. In the spring, high concentrations of SO_2 in the residential area, Yaeum, were observed when the southeast wind was in force. There are petrochemical complexes in the southeastern part of Yaeum, where the SO_2 emitted from the petrochemical complexes contributes to the high concentrations in the residential area. The pollution sources related to the top 5–15% SO_2 concentration results at Yeocheon were indicated to be close to the petrochemical complexes, and the sources related to the top 5% the SO_2 concentration results were the nonferrous industrial complexes. The SO_2 levels in the roadside areas were affected by the industrial complexes located toward the east and southeast. In addition, automobile emissions were considered to be one of the sources of high levels of SO_2. In summer, the top 5–15% SO_2 concentration results were influenced by strong winds from the south and the southwest, and the top 5% the SO_2 concentration results were influenced by the wind from the south. This means the pollution sources were located in the south, which was expected considering the location of the nonferrous industrial complexes. The high SO_2 concentration in Yeocheon showed a similar pattern in the CBPF plot in spring, and it was influenced by the surrounding petrochemical complexes. The top 5% of the SO_2 concentration results indicated that the location of major sources were the nonferrous industrial complexes. The SO_2 level in the roadside areas was similar to that in the case of Yaeum in summer, which was influenced majorly by sources located on the southern side. The local sources of high levels of SO_2 in the residential areas during autumn were predicted to be similar to those in the case of summer, that is, the southern and southwestern regions were the sources of pollutants. Unlike in the spring and summer, the top 5–15% concentration results and the top 5% concentration results at Yeocheon were affected by only the surrounding petrochemical industrial complexes, especially in the eastern and northern regions. The results of the roadside areas were not very different from those obtained in the case of summer. The SO2 concentrations in winter at all sites showed different patterns from the cases of spring, summer, and autumn. The SO_2 concentration at Yaeum indicated that most of the wind originating from the south toward the east showed high levels. The top 5–15% of the SO_2 concentration results in Yeocheon were observed to be influenced by the east, while the top 5% of the concentration results were influenced by a strong wind from the west. This was expected to occur owing to the wind blowing from residential areas and nonferrous industrial complexes rather than the effects of nearby petrochemical industrial complexes. The high SO_2 concentration in the roadside areas was observed when strong south winds and southeast winds were in force, and it was affected not by emissions from surrounding vehicles but by the nonferrous and petrochemical industrial complexes (Figure 27).
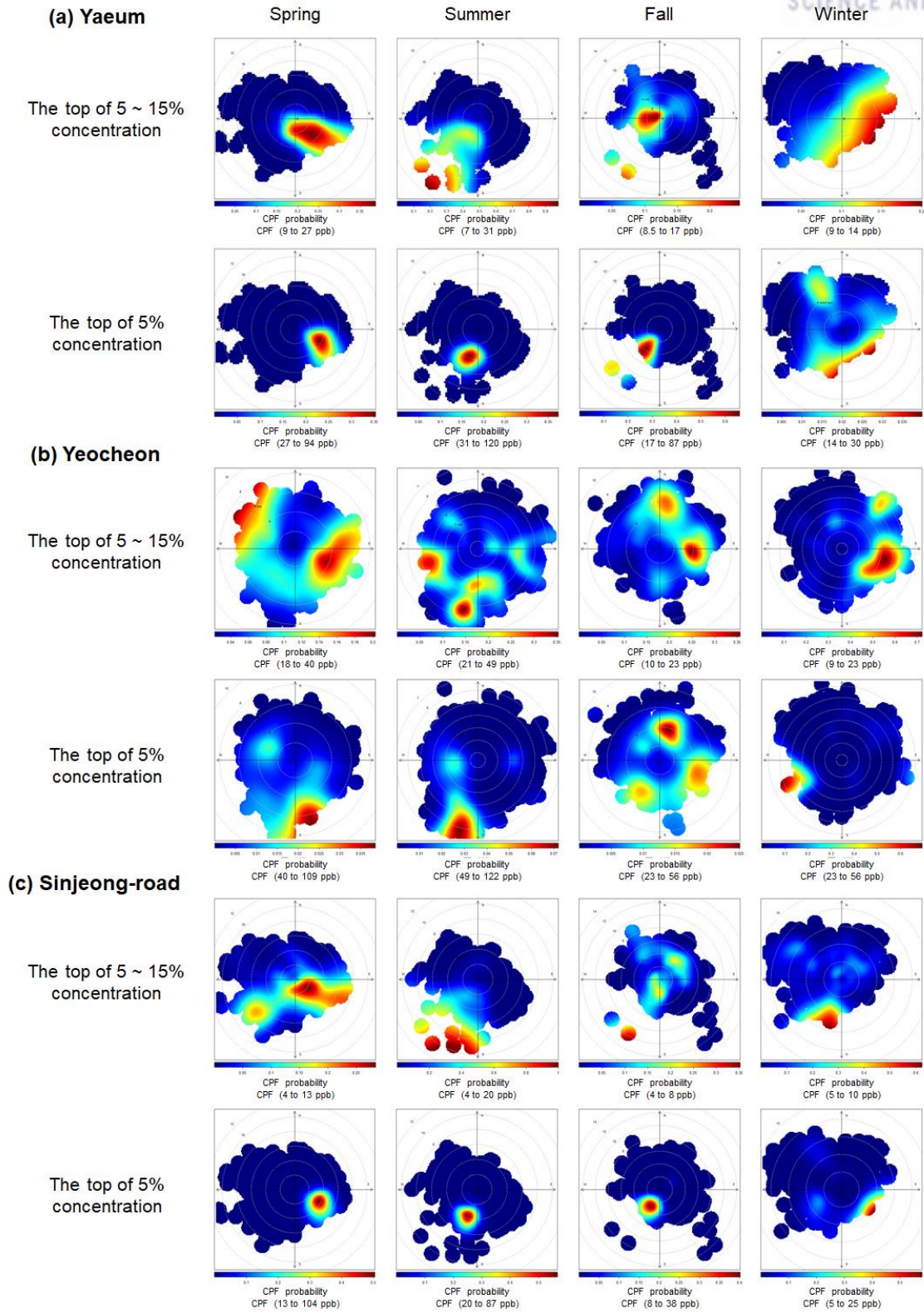
Figure 27. CBPF plot indicating top of 5~15% and 5% concentration of SO_2 in the three sites

3.2.4 Surface wind field in Ulsan

The CALMET model was used to calculate the surface wind field of Ulsan city on monthly and seasonal bases. First, in the case of spring, the most of wind was from the north, and some wind from the south blew west of Ulsan. In the industrial area located along the southeast coast, the wind blew toward the south along the coastline and escaped to the East Sea south of Ulsan. The wind passed through the automobile, petrochemical, and nonferrous industrial areas in that order and then escaped to the East Sea. The wind in the urban areas blew southward as well. The wind pattern between the downtown and the industrial areas in spring showed that the PM_{10} generated by the downtown area, as well as the petrochemical and automobile industrial complexes affected the southern part of Ulsan. Moreover, the air pollutants discharged from the nonferrous industrial complexes escaped toward the East Sea. These winds were expected to reduce the impact of industrial emission on residential areas (Figure 28).

The wind pattern in the summer was the opposite to that in spring, which was dominated by the southeastern wind blowing from the sea toward the land. Air pollutants emitted by the petrochemical and nonferrous industrial complexes directly affected the urban areas. Even in the east of Ulsan, westward wind blew, so air pollutants from the automobile and the shipbuilding industrial complexes were expected to influence the downtown area (Figure 28).

Since most of wind in the fall blew from the north, except the mountainous region located in the western part of Ulsan, it was expected that the air pollutants emitted by industrial area in Pohang City, located north of Ulsan, would affect the pollution levels in Ulsan (Figure 28).

In the winter, northwest winds blew in Ulsan similar to those in the spring. The difference was that the northwest wind blew over the entire area, including the western part, so the wind around the industrial complexes in the southeastern part was directed toward the East sea. The effects of most of the pollutants emitted from the industrial complex on the downtown area were expected to decrease (Figure 28).
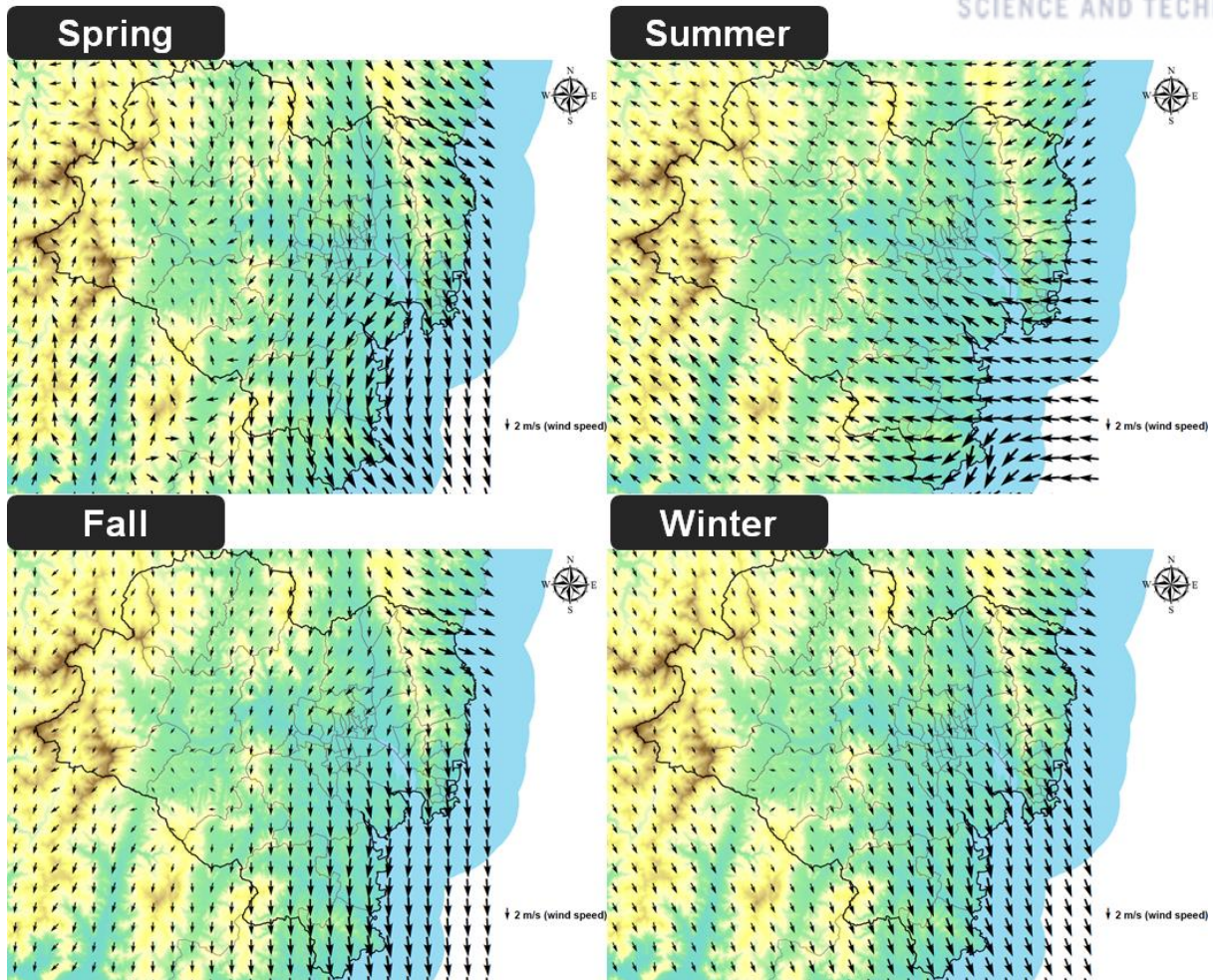
Figure 28. Seasonal surface wind field of Ulsan in 2012 derived by CALMET

From January to March, almost all of the wind was along the northwest direction, and the wind speed was relatively strong in the coastal area. In April, the southwestern wind blew from the land toward the East Sea northeast of Ulsan. From May, the wind speed decreased, and it was directed inland from the coastal area, which is characteristic of the northeast winds. However, the wind in western part of the city was directed toward the northwest. The results in June were similar to those in May, and wind speed was slightly stronger. From July, the speed of the southward wind decreased over the entire region, meaning that wind blew directly from the industrial area toward the downtown area. In August, south-easterly winds and easterly winds blew in a direction similar to that of the July wind, which passed from the industrial area toward the downtown area. From September, this wind was converted into a north wind. Similarly, wind blew along the coastline in October. In November and December, northwesterly wind was the dominant component (Figure 29).
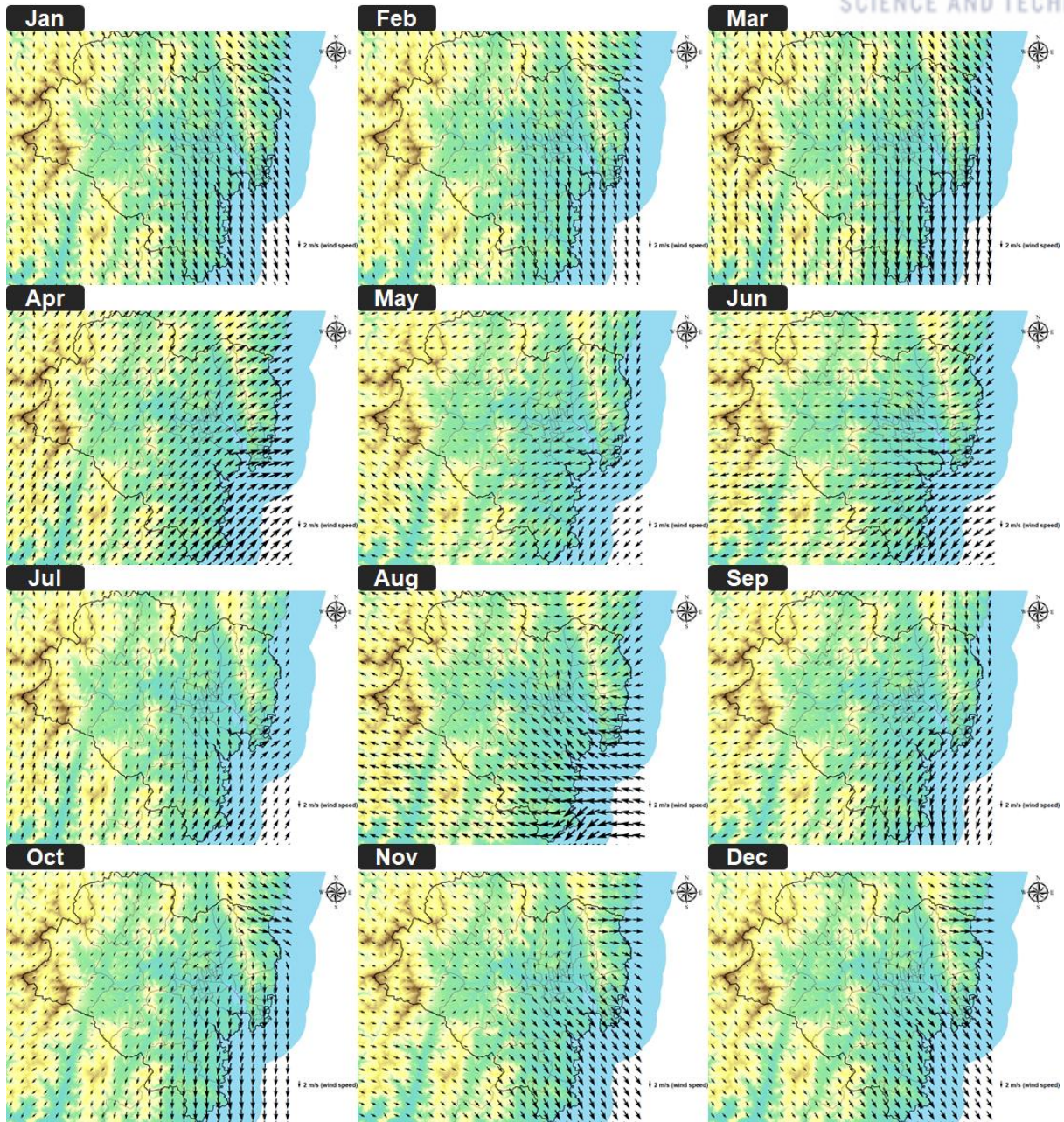
Figure 29. Monthly surface wind field of Ulsan in 2012 derived by CALMET

In the daytime, surface wind blew in a direction opposite to that in the nighttime (Figure 30). The representative times of day and night were selected as 12:00 PM and 0:00 AM, respectively. In the nighttime, northwesterly wind was the main component, and the western part of Ulsan showed weak average wind speed. The wind in the middle region of Ulsan blew from the urban area toward the petrochemical and nonferrous industrial complexes. By contrast, the east wind was dominant during the daytime. The average wind speed was stronger than that at night, so it was expected that air pollutants emitted from the eastern industrial complexes affected the urban area.

The previous 3.2.2 study (Relationship between PM_{10} and SO2 hourly concentration) showed that SO_2 levels in the residential and roadside areas were higher than the PM_{10} levels in the daytime. Because the daytime surface wind blew from the residential toward the industrial areas, SO_2 levels in the residential and roadside areas were expectedly influenced by the industrial complexes. Conversely, the PM_{10} level was expected to be affected by other sources, not industrial complexes.
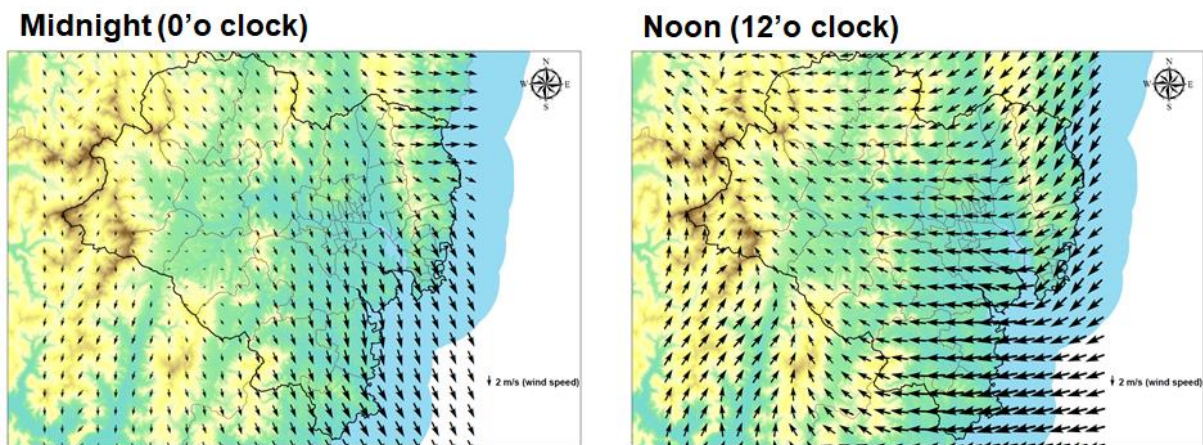
Figure 30. Surface wind field by the time, nighttime (00:00 AM) and daytime (12:00 PM)

3.2.5 CALPUFF result of PM_{10} and SO_2 emission

The CALPUFF model was used to simulate on as monthly basis the surface wind field created using CALMET. First, PM_{10} was mostly emitted from point sources in the petrochemical complexes, and these sources had the greatest effect on Ulsan compared to the other point sources. From January to March, the PM_{10} emitted from the petrochemical industrial area dispersed toward the southeast, meaning the pollutants moved toward the East Sea. From April, PM_{10} dispersion toward the East Sea declined. The high level of PM_{10} emitted by the petrochemical complexes affected the eastern part of Ulsan (Dong-gu) and the nonferrous industrial complexes located eastward. In May, the impact on the east decreased compared to that in April, but it still tended to spread inland. From June to August, the tendency of dispersion from the petrochemical complexes toward the downtown area was strong, and additionally, in August, the pollutants tended to spread toward the northeast part. From September to December, PM_{10} was dispersed toward the East Sea. Overall, in all seasons, except summer, pollutants were spread out toward the East Sea, and in summer alone, PM_{10} was strongly dispersed in the residential areas (Figure 31).

In the case of SO_2 dispersion, unlike PM_{10} emissions, the two main sources were petrochemical and nonferrous industrial areas. Between the two, the nonferrous complexes dominated SO_2 emission, and the diffusion tendency was more distinct. In January and February, high concentrations of SO_2 were dispersed from the nonferrous industrial complexes toward the East Sea according to the seasonal wind. In March, April, and May, SO_2 was dispersed toward the East Sea, and along the northeast and south directions, affecting not only the eastern part but also the southern part of Ulsan. In addition, the influence of petrochemical complexes was confirmed to decrease in May. The tendency of SO_2 to disperse toward the East Sea decreased sharply in June; by contrast, SO_2 mainly affected urban areas. The effects of petrochemical and nonferrous industrial complexes were similar to each other in July and August. From September to December, it dispersed again toward the East Sea. Unusually, in October, the diffusion of high concentrations of SO_2 in air influenced the automobile industrial areas, and in December, the influence of the petrochemical complexes increased (Figure 32).
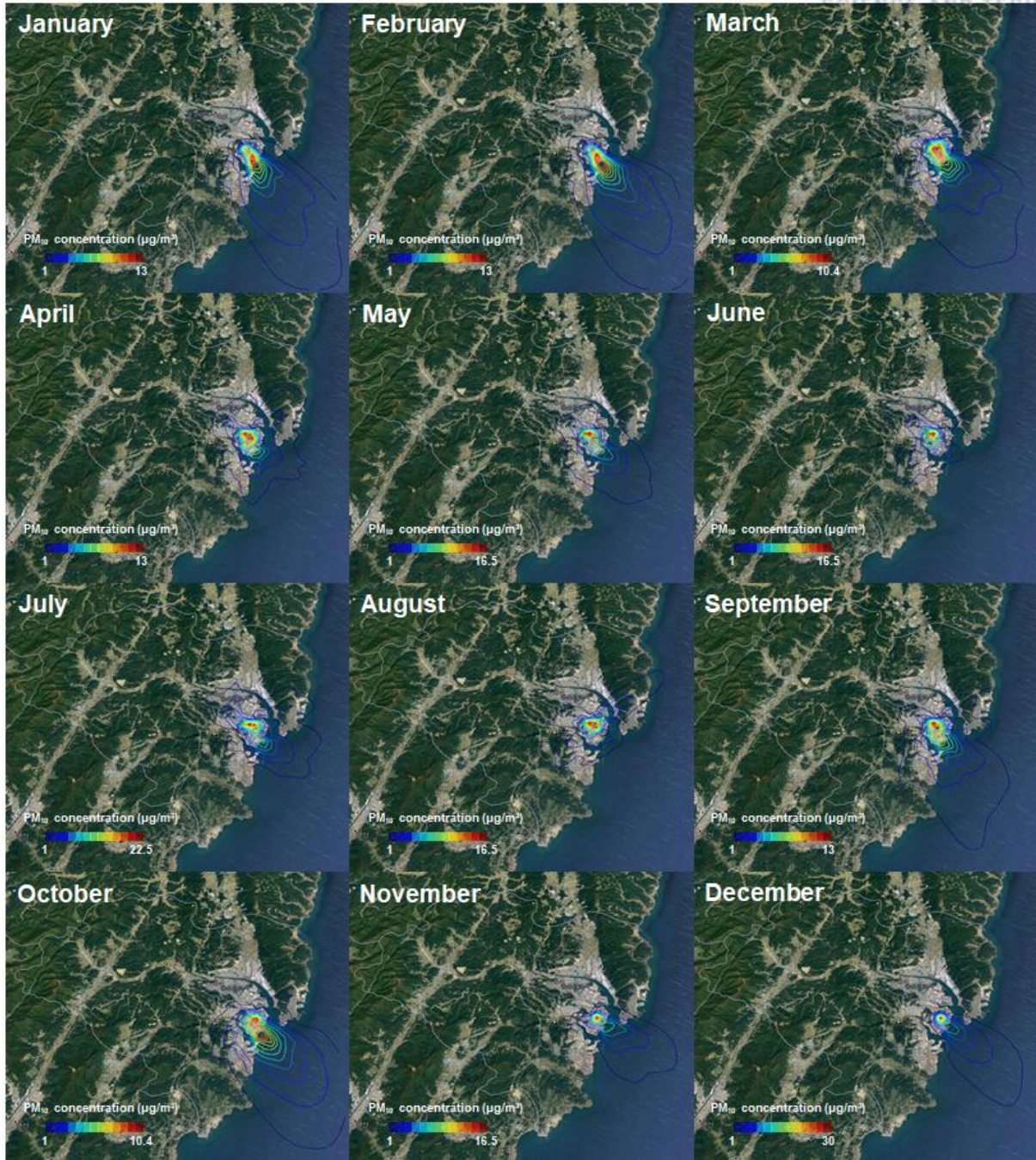
Figure 31. Monthly PM$_{10}$ dispersion from point sources in Ulsan by simulating CALPUFF
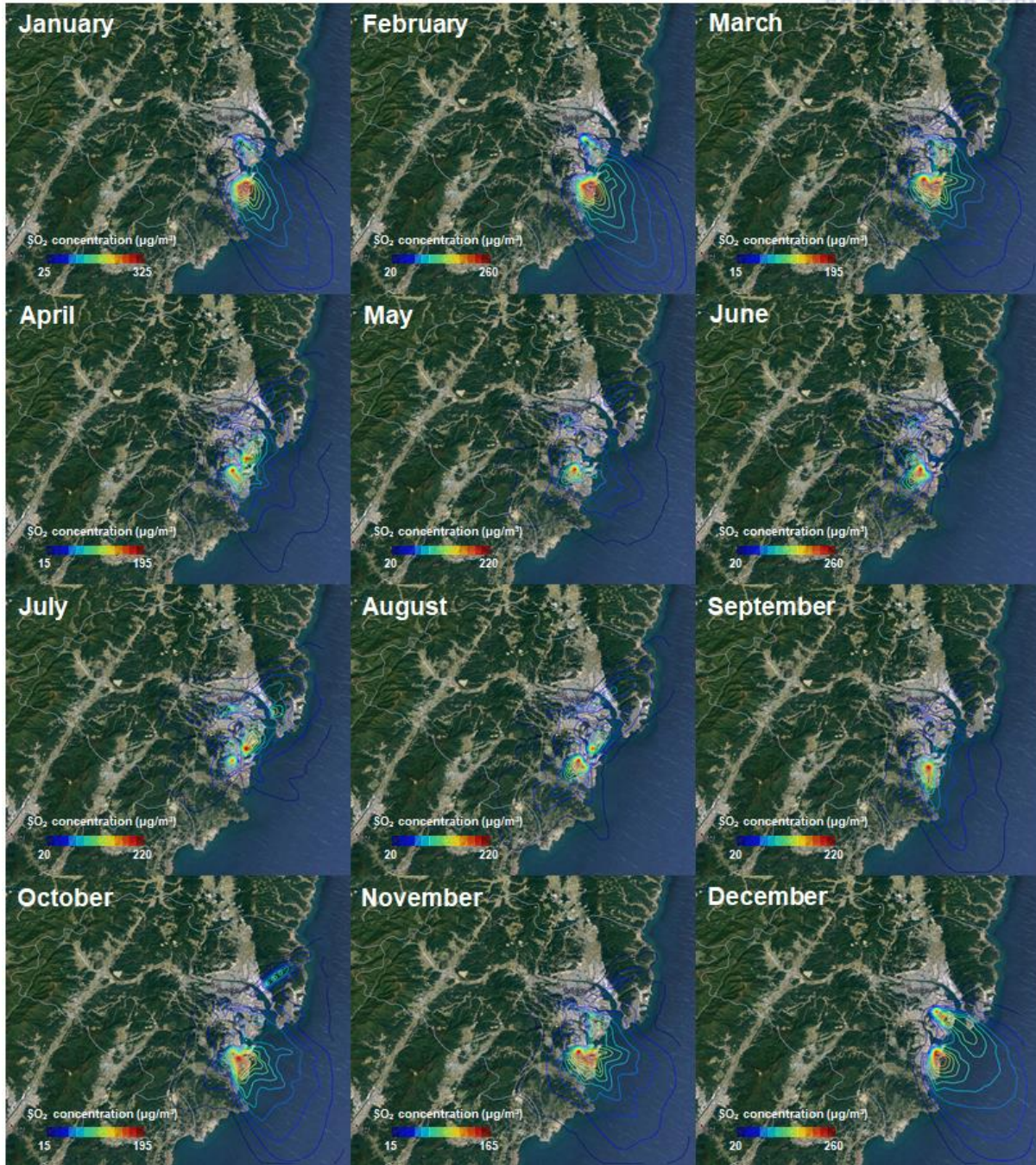
Figure 32. Monthly SO₂ dispersion from point sources in Ulsan by simulating CALPUFF

The monthly average PM_{10} concentration derived using CALPUFF showed that all three sites increased until July and then decreased until December. Totally, The PM_{10} levels were high in summer. This means that the influence of the point sources in the industrial complexes was the strongest during April to August. The residential areas and the roadside areas (Yaeum and Sinjeong-road) showed the highest peaks in June and July, and Yecheon showed the highest peak in April and May. The difference in level between summer and the other seasons was 2–10x in the case of the residential and the roadside areas, but it was smaller in the case of Yeocheon, the industrial area (Figure 33 (a)).

The monthly average concentration of SO_2 derived using CALPUFF was different from that of PM_{10}. The residential and the roadside areas showed the highest peaks in June and July, as in the case of PM_{10}, but the highest peak in Yeocheon was in July and August, which is different from that in the case of PM_{10}. It appeared that Yeocheon, located in the petrochemical complex, was affected by the dispersion of SO_2 from the nonferrous industrial areas in July and August. Same as the case of PM_{10}, the difference between summer and the other seasons was large in Yaeum and Sinjeong-road, and the difference in pollutant concentration between the seasons in Yecheon was smaller than that at the other two sites (Figure 33 (b)).
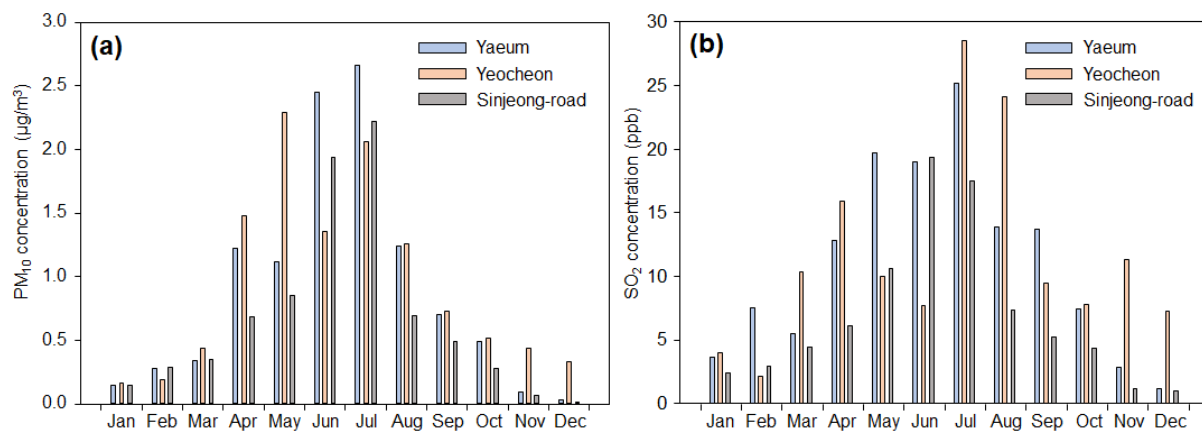
Figure 33. Monthly concentration of (a) PM_{10} and (b) SO_2 derived by CALPUFF model

The daily average concentration distribution derived from CALPUFF can be used to obtain the detailed variation in concentration in each area due to the point sources. Unlike the monthly average concentration determined by modeling, the daily variation of modeling concentration clearly showed the difference of each day, regardless of the influence of the point source. Since the CALPUFF model

was used to simulate only point source emissions, which differed considerably depending on the direction of the wind, the standard deviation of the daily concentration was high.

The daily concentration of PM_{10} and the frequency of peaks at the Yaeum site increased during April to September, especially in June and July (Figure 34 (a)). The peak distribution of PM_{10} concentration at Yeocheon appeared mainly from April to September. High peaks were observed in May and June, and these were generally higher than those at the other two sites ((Figure 34 (b)). The peaks of the modeled PM_{10} concentration in the Sinjeong roadside area increased from April to August, and the highest peaks appeared in June and July. Compared to the other two sites, the average concentration and peak frequency at this site were lower (Figure 34 (c)).

Figure 34. Daily concentration of PM_{10} at (a) Yaeum, (b) Yeocheon, and (c) Sinjeong-road sites derived by CALPUFF model

The result of the daily SO_2 concentration at Yaeum was different from that of the PM_{10} case. The peak frequency was high from April to September, as in the case of PM_{10}, but the SO_2 levels in spring were similar to those in summer. Unlike PM_{10}, because SO_2 emissions were influenced not only by the petrochemical industrial complexes but also by the nonferrous industrial complexes, seasonal differences were smaller than those in PM_{10}, and peak frequencies were higher (Figure 35 (a)). Daily SO_2 level in Yeocheon remained at the highest level until December. Peaks appeared in July and August because the SO_2 emitted by the nonferrous industrial area dispersed toward the northeast in July and August, affecting the petrochemical industrial area. The peaks in October, November, and December were high owing to the increase in SO_2 emission by the petrochemical industry compared to that in the other seasons, and the pollutants were dispersed toward the northeast (Figure 35 (b)). Only the Sinjeong roadside showed similar PM_{10} results among the three sites. Based on this result, we interpreted that the influence of PM_{10} and SO_2 on the roadside areas was lower than that on the industrial areas (Figure 35 (c)).

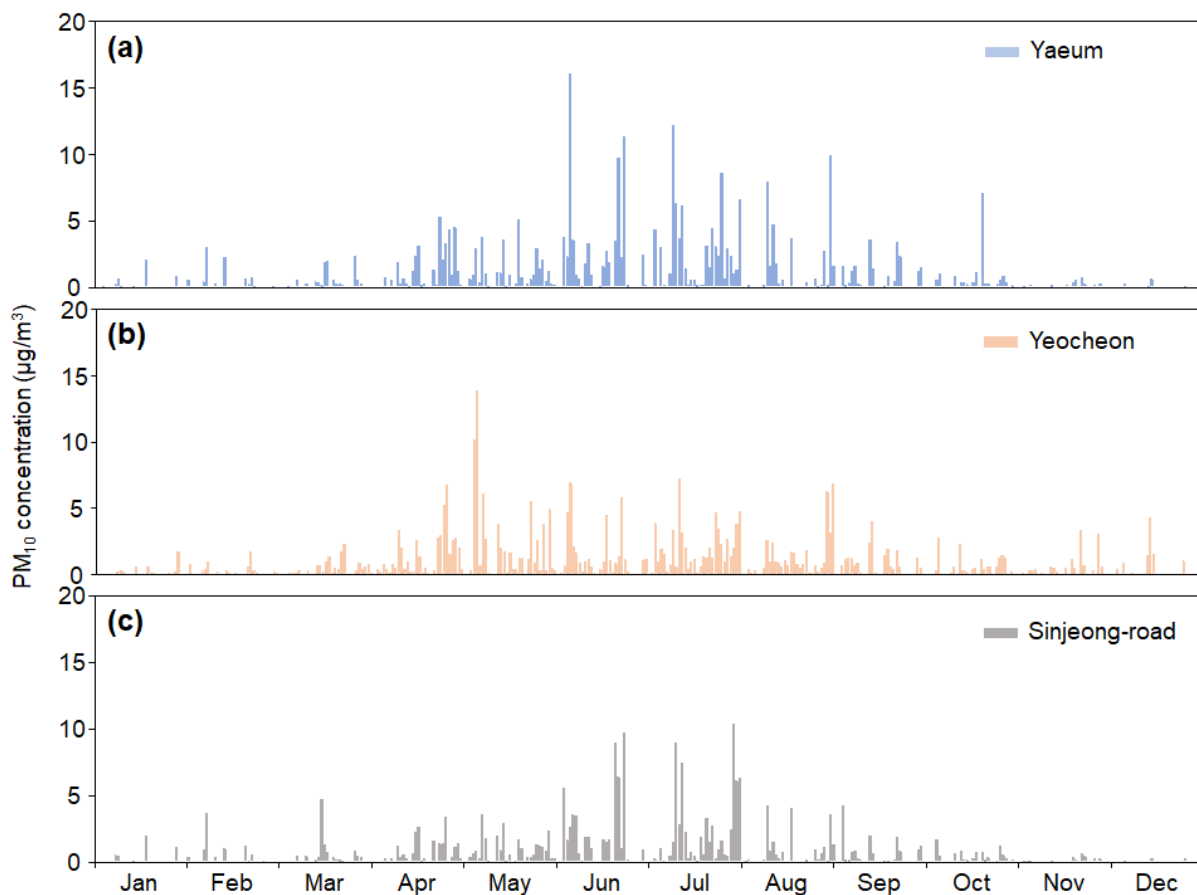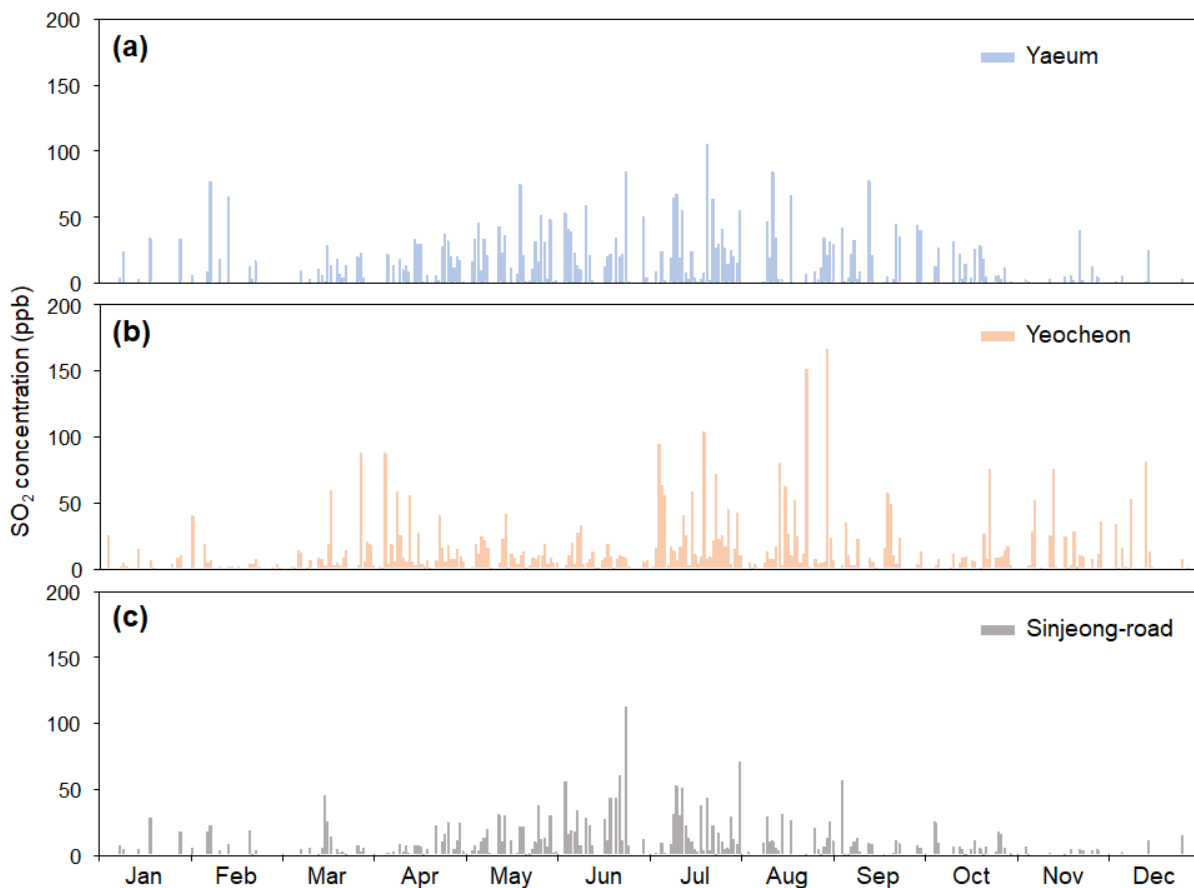

Figure 35. Daily concentration of SO_2 at (a) Yaeum, (b) Yeocheon, and (c) Sinjeong-road sites derived by CALPUFF model

47

The influence of the point sources on pollutant concentration as determined using the CALPUFF model were compared with the concentration values measured by the monitoring stations. For PM_{10}, the concentration determined using CALPUFF was lower than the monitored value because the amount of emission from the point sources was about 19% of total PM_{10} emissions in Ulsan. Even in residential areas, the modeled values of the point sources were smaller than the actual measured value because the distance from the residential area to domestic sources and mobile sources were smaller than the corresponding distances to the industrial point sources. In addition, the values calculated using CALPUFF were lower than those obtained using the other dispersion model AERMOD (Dmitry et al., 2016).

A comparison of the modeled and monitored values of PM_{10} in the residential areas showed that the monitored value increased in spring and decreased in summer but the modeled value increased in summer. This indicated that the effect of industrial emission increased in summer but the effect of LRAT and other local sources was strong in spring. However, the monitored and modeled concentrations increased in June and July and decreased again in August. Based on this finding, we interpreted that CALPUFF simulated well the variation in PM_{10} levels due to the influence of the industrial complexes in summer (Figure 36 (a)).

A comparison of the monitored and modeled values of PM_{10} in the industrial area showed that the variation in PM_{10} levels between the two sets of values was similar. Based on this finding, we interpreted that the concentration value was largely influenced by other sources such as LRAT, but the dispersion pattern related to industrial sources was well simulated (Figure 36 (b)).

In the roadside area, the pattern of the modeled values was similar to that in case of the residential area, but the variation in the monitored value was constant compared to that in the other areas. This indicated that the level of PM_{10} in the roadside area was influenced to a smaller extent than those in the residential and industrial areas (Figure 36 (c)).
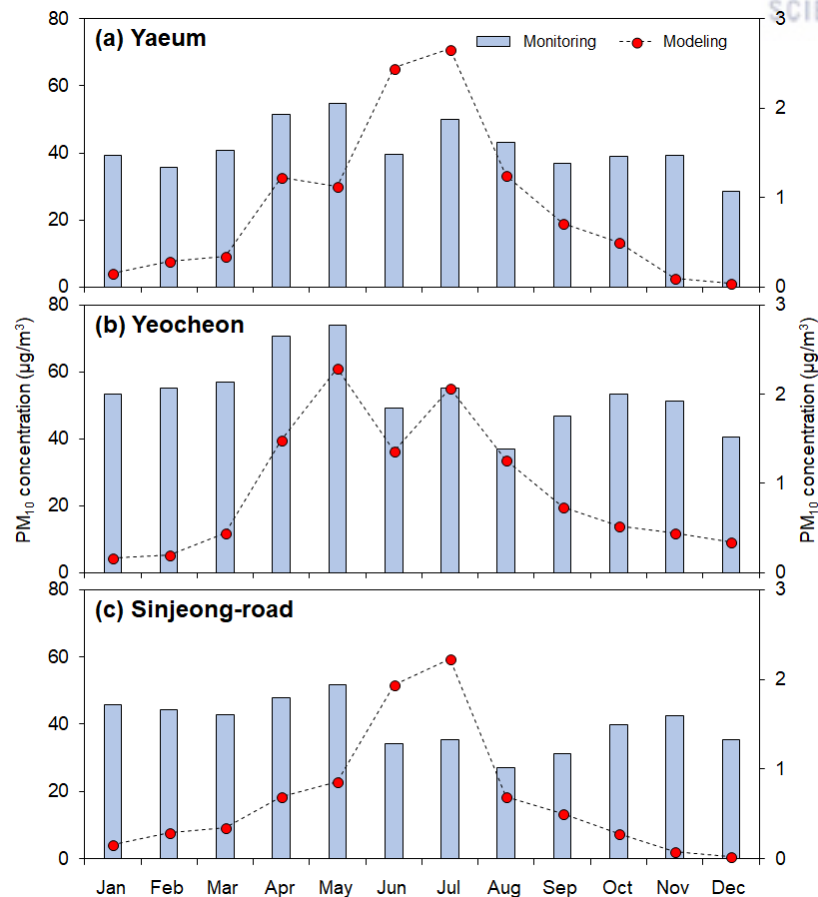
Figure 36. Monthly variation of PM_{10} by monitoring and modeling at (a) Yaeum, (b) Yeocheon, and (c) Sinjeong-road site

The amount of SO_2 emission from the point sources used in the CALPUFF simulation was approximately 80% of the total SO_2 emissions in Ulsan. Unlike the underestimated modeling result of PM_{10} level, the modeled SO_2 values were similar to the monitored values. Except for the industrial area, the residential area and the roadside area showed overestimation of the modeling results in summer.

The modeled values of SO_2 at Yaeum were overestimated related to the monitoring values in summer. However, the variation of concentration during March to September was similar between the monitored and modeled values. Similar to case of PM_{10}, the modeled values were lower than the monitored values in winter. This was ascribed to the effect of SO_2 emissions due to residential heating rather than the emission effect of the industrial complexes in winter. Overestimation of the modeled values in summer was not considered the effect of the building block in air dispersion model and the facility which reduced SO_2 in the residential area itself. The overestimation was ascribed to calculation of the effect of the SO_2 emitted from industrial stacks on the residential areas (Figure 37 (a)).

In the case of Yeocheon, the modeled and monitored values were similar in terms of variation and concentration level, except for the results obtained in January and February. In January and February, the modeled values were underestimated owing to the effect of combustion of fuel for domestic heating. In the other periods, the results of SO_2 dispersion simulations were good (Figure 37 (b)).

The SO_2 result obtained at the Sinjeong roadside site was the same as the PM_{10} result. The variations in the modeled and monitored results were different. The reason was not only the effect of the industrial complexes but also the effect of surroundings, such as vehicular emissions. The overestimated period was interpreted as the same reason as the case of the residential area (Figure 37(c)).
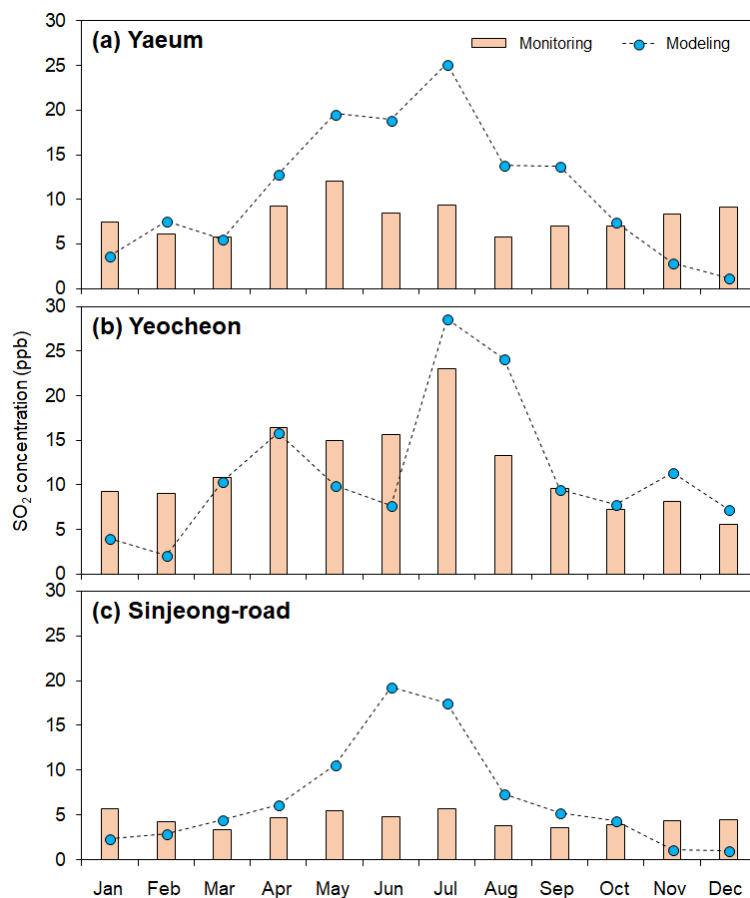
Figure 37. Monthly variation of SO_2 by monitoring and modeling at (a) Yaeum, (b) Yeocheon, and (c) Sinjeong-road site

3.3 Long-range atmospheric transport of PM_{10}

3.3.1 Backward trajectory analysis result

It is well known that air pollutants in China affect not only Korea but also Japan due to LRT (Toshihiko et al., 2002). Even the PM_{10} among the CAPs transported from Mongolia also affected to East Asia (Chung, 1992; Kim and Park, 2001; In and Park, 2002). Unlike SO_2, PM_{10} was considered the LRT effect because lifetime in troposphere was several weeks. The backward trajectory analysis results were interpreted to identify the long-range transport pattern of air mass in Ulsan.

In January and February, all backward trajectories came from the eastern part of China. Even some backward trajectories came from Mongolia and Russia. During March to, the number of backward trajectories from the East Sea and the Pacific were increased as well as from China. Most backward trajectories during June to August came from Japan and the South Sea. The backward trajectories in September showed a phenomenon of staying around in the East Sea. Then, most of the backward trajectories after October came again from China like the case of January and February (Figure 38).

Figure 38. The monthly pattern of backward trajectories in 2012 Ulsan

3.3.2 Cluster analysis result

In chapter 3.3.1, the backward trajectory was interpreted according to temporal classification (monthly, seasonally). However, in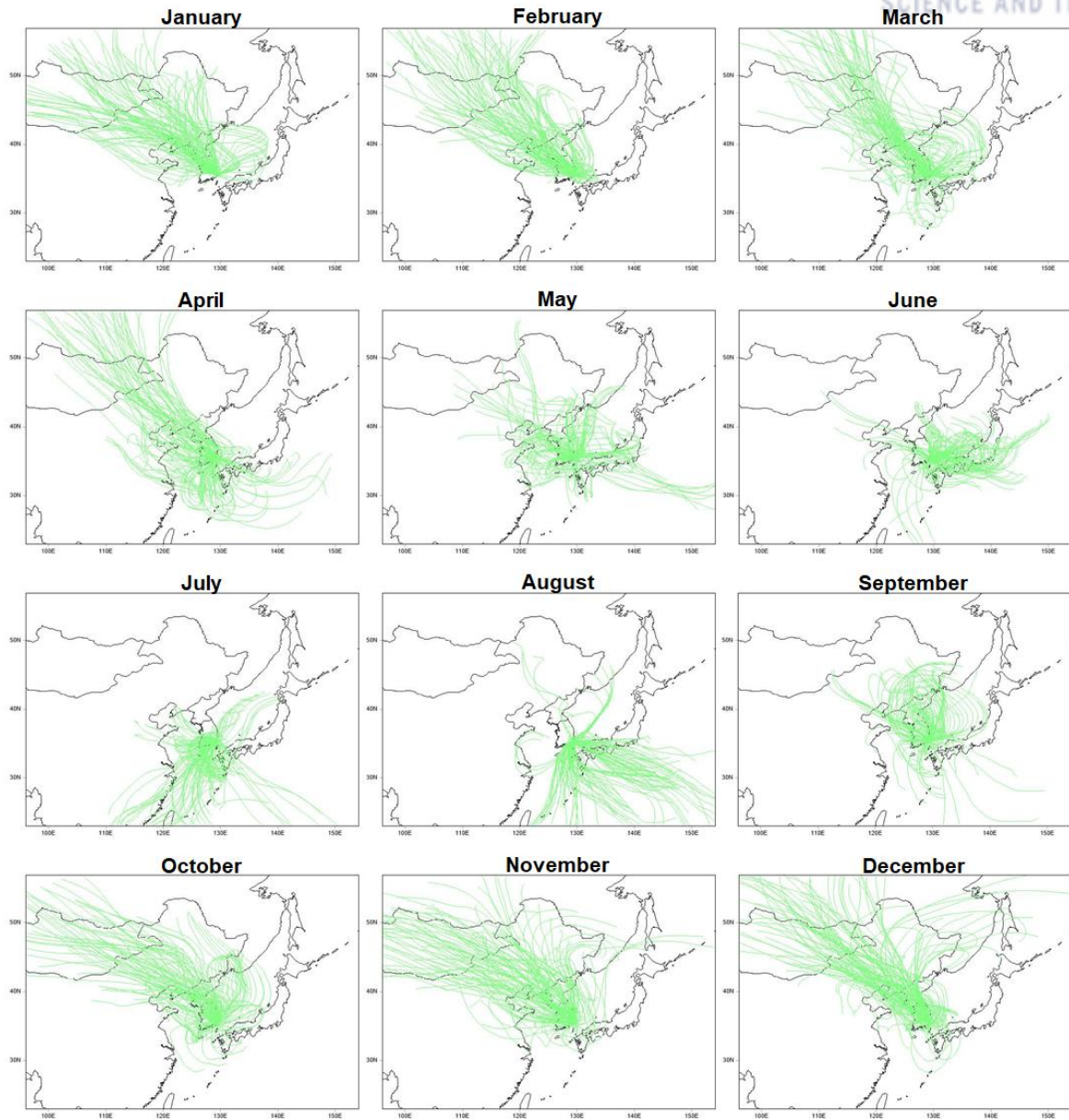 addition to temporal classification, a statistical classification method called cluster analysis was used to interpret the LRAT of PM_{10}.

The first cluster of the backward trajectories was indicated to originate from the northwest side of Ulsan. A total of 496 backward trajectories ranked of the second-largest number of trajectories in 2012, which accounted for 34% (Figure 39 (f)). The backward trajectories passed through toward North Korea from the east of China, even Mongolia, and they were influenced by the industrial and residential areas located in Shenyang, as well as North Korea. Even the backward trajectories of this cluster were expected to be influenced by the sandstorms originating from the Gobi desert in Mongolia and by biomass burning in North Korea (Figure 39 (a)).

The second cluster of backward trajectories was the nearest to the Korean East Sea. These backward trajectories stayed near the East Sea and moved around South Korea. This indicated the influence of PM_{10} sources in the large cities and industrial cities of South Korea rather than the LRAT effect (Figure 39 (b)). The number of trajectories in second cluster was 534, accounting for 36% and representing the largest percentage of all clusters (Figure 39 (f)).

The third cluster of backward trajectories originated from the westside of Ulsan, which was influenced by of the industrial areas of Beijing and Tianjin in China, as well as the western part of South Korea, as the LRAT effect. A few backward trajectories in the third cluster indicated the influence of PM_{10} from Shanghai (Figure 39 (c)). The number of trajectories in third cluster were 136, accounting for 9% (Figure 39 (f)).

The fourth cluster of backward trajectories included those originating from the southside. They showed the impact of the Pacific Ocean and of Shanghai, which is in the southeastern part of China (Figure 39 (d)). The number of trajectories in the fourth cluster was 214, accounting for 15% (Figure 39 (f)).

The last cluster of backward trajectories originated mostly from Japan. The backward trajectories in this cluster indicated the influence of the southern part of Japan, including the influence of the Kitakyushu industrial area in the Kyushu region in the southern part of Japan (Figure 39 (e)). The number of

backward trajectories in this cluster was 84, accounting for 6%; this cluster was the smallest among the

other clusters (Figure 39 (f)).
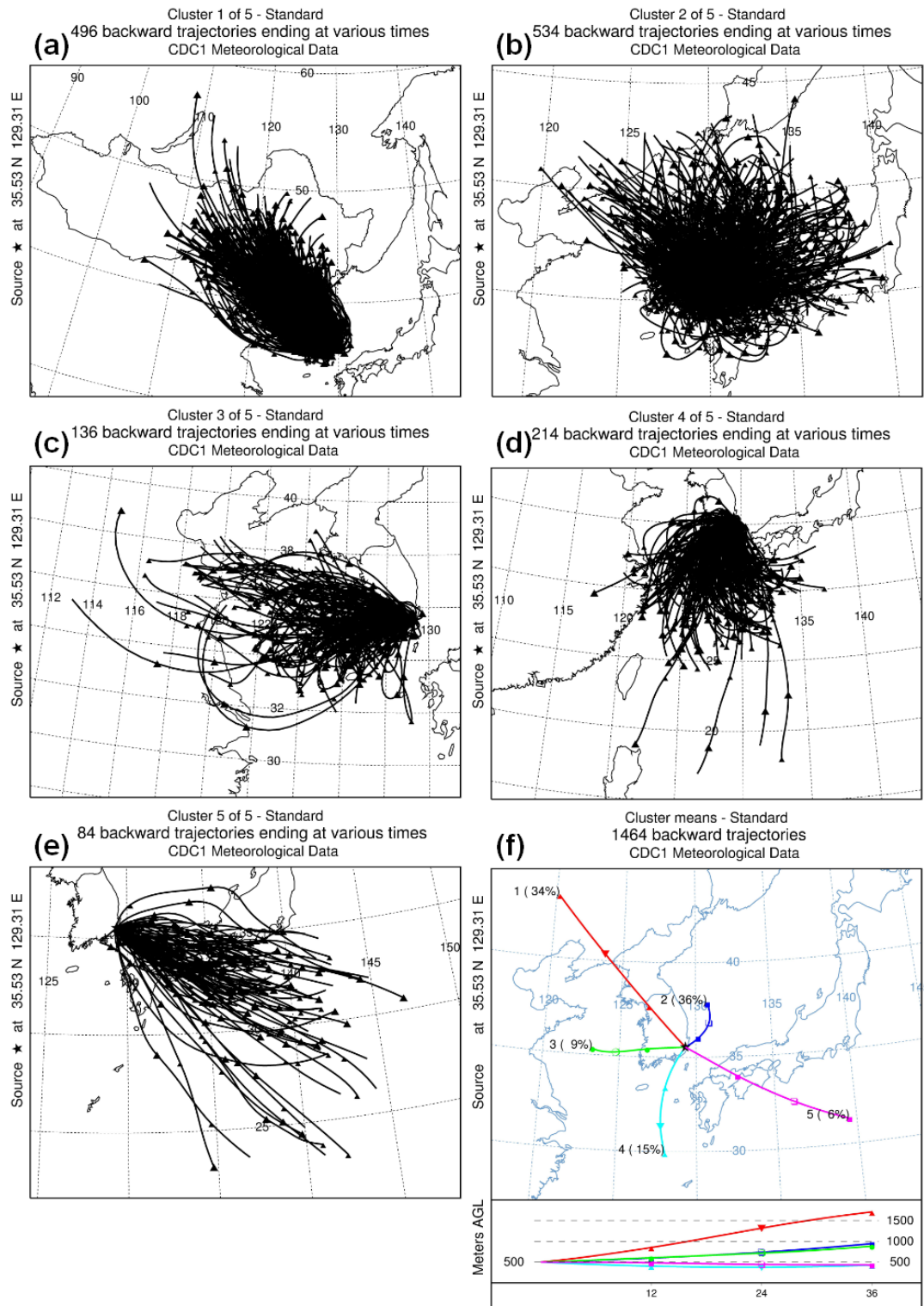
Figure 39. The result of cluster analysis in Ulsan considered five groups

3.3.3 Potential soucre contribution function result

PSCF was simulated seasonally with backward trajectories and hourly PM_{10} concentration data. Seasonal comparisons of the PSCF in 2012 were made to identify the sources of high concentrations and the frequency of the high-concentration phenomenon. The pollution criterion of concentration was set as the top 25% of the results of PM_{10} level in 2012, which was 56.67 μg/m^3.

First, in spring, high concentrations PM_{10} were confirmed to have originated from the West Sea, as well as from Qingdao, Beijing, and Tianjin in China. There were more yellow and red cells compared to those in the other seasons, indicating a high concentration of PM_{10} was present in spring (Figure 40(a)). In summer, the southeastern part of South Korea and the West Sea were the potential sources of high concentrations of PM_{10} (Figure 40(b)). In autumn and winter, the backward trajectories originated mostly from China, but they were not potential sources of high concentrations of PM_{10} (Figure 40 (c), (d)).

Figure 40. PSCF plot in Ulsan during (a) spring, (b) summer, (c) fall, and (d) winter

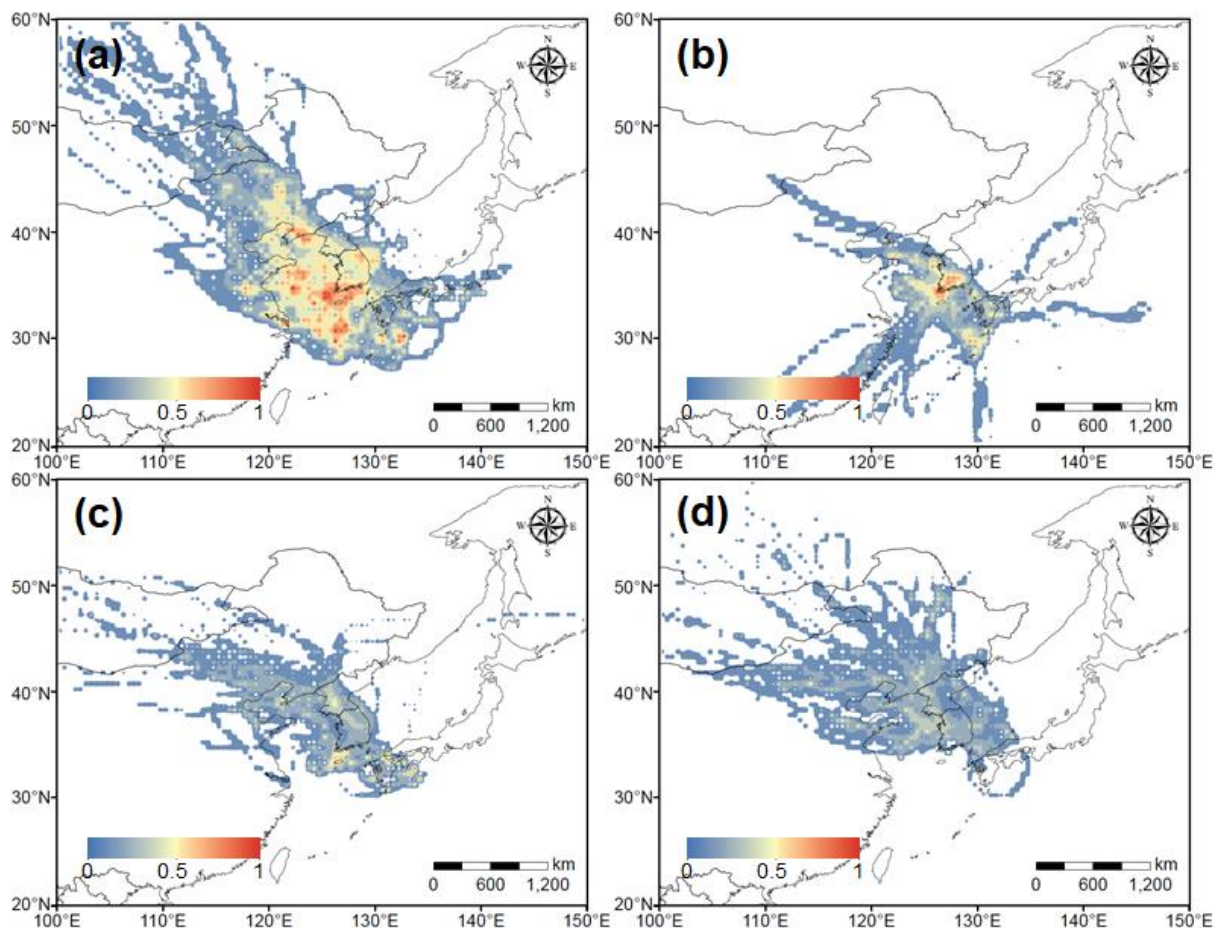PSCF was applied to the results of cluster analysis as well as to seasonal PSCF. The top 75% of the concentration results for each of the five clusters was used as a pollution criterion value, and this concentration value indicated the locations of the sources in each cluster.

Most of the potential sources in Cluster 1 were in eastern China, including Shenyang, and some in Mongolia. The average PM_{10} concentration in the back trajectories included in Cluster 1 was 45.29 $\mu g/m^3$, which was higher than the average concentration in 2012. In fact, in the Mongolian area, there were many dusts from the desert, such as Asian dust, but there were few anthropogenically generated PM_{10} sources (Figure 41 (a)).

The second cluster indicated that the potential sources were in the Gyeonggi province, some parts of North Korea, and most of South Korea. Cluster 2 represented domestic sources. The average concentration was 42.52 $\mu g/m^3$, which was lower than that of Cluster 1 (Figure 41 (b)).

Cluster 3 showed potential sources of PM_{10} in the Beijing and Tianjin industrial areas, including the West Sea. The average concentration of the backward trajectories in Cluster 3 was 57.08 $\mu g/m^3$, which was the highest among all clusters. This indicated that the highest concentration of PM_{10} occurred when the backward trajectories originating from the Beijing and Tianjin Industrial areas were in force. In fact, Beijing and Hebei in China emitted high amounts of PM_{10} in China, and the trajectories from these regions were expected to have the greatest impact on Ulsan (Figure 41 (c)).

The backward trajectories in the fourth cluster were mainly contaminated by the South Sea and Shanghai, which is in the southeastern part of China. The average concentration was 52.24 $\mu g/m^3$, which was the second highest concentration among all clusters. This indicated that Shanghai was a high-PM_{10} source, and it affected Ulsan (Figure 41 (d)).

The last cluster showed a potential source of PM_{10} in southern part of Japan. The average concentration was the lowest among all clusters, 33.34 $\mu g/m^3$. The PM_{10} concentration affected by LRAT from Japan was the lowest (Figure 41 (e)). The PSCF of the entire period showed that most of the PM_{10} due to LRAT originated from the region surrounding the West Sea and China (Figure 41 (f)).
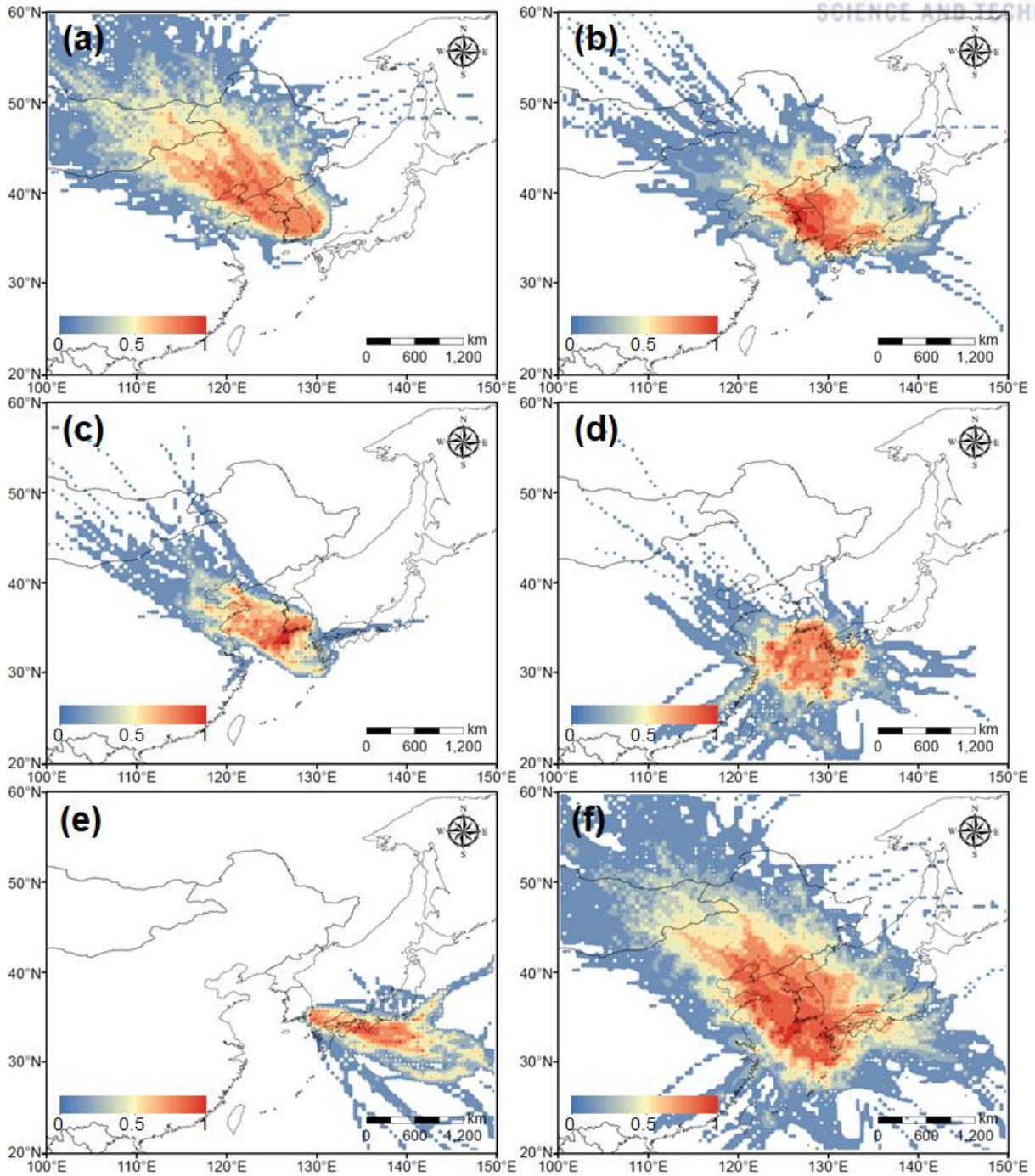
Figure 41. PSCF plot in Ulsan based on trajectories of (a) cluster 1, (b) cluster 2, (c) cluster 3, (d) cluster 4, (e) cluster 5, and (f) total trajectories

3.4 Importance factor of PM_{10} and SO_2 concentration

The importance was calculated according to each factor, and the importance of the factors was determined through relative comparison. In this study, pollutants emitted from the stacks in industrial complexes were selected as a factor of local pollution sources and the results of cluster analysis were selected as a factor of LRAT influence. Other factors (temperature, wind speed, wind direction, precipitation) were selected as meteorological factors (Liew and Wiener, 2018).

In previous results such as CBPF, CALPUFF, cluster analysis, sources of PM_{10} were hard to identify how much influence it had, and which influence it had. However, in the result of RandomForest, temperature was the most important factor. Temperature was indicated a contributing factor to the dispersion and secondary generation of local pollution and represented a complex source. It means that the main source of annual average PM10 level in Ulsan was more affected by complex pollutants and secondary aerosol than pollution by factory discharge and long-distance effect. In addition, the effects of industrial complex emissions and LRAT effect were the second most important factors. The effects of industrial complex emissions and long-distance effect were also important sources of PM_{10} pollution in Ulsan City (Figure 42).

In the results of CIT, nodes 14 and 16 were classified as the highest PM_{10} concentration groups. These high concentration groups were shown when the temperature was high, it was affected by cluster 3 and 4 (Beijing, Tianjin, and Shanghai), and the influence of the industrial complexes were large (Figure 44). In other words, the concentration of PM_{10} in Ulsan was highest when the effect of temperature and LRAT and the emissions from industrial complexes were all affected.

The effects of industrial complexes were the main source of SO2 derived from the previous CBPF and CALPUFF results. The results of RandomForest also showed that the industrial emission was a much more important factor (Figure 43). The atmosphere in Ulsan was polluted by SO_2 emitted from the chimney in the industrial complex. To solve this problem, it is necessary to seriously consider the emission from the industrial complex.

Conditional importance of variables
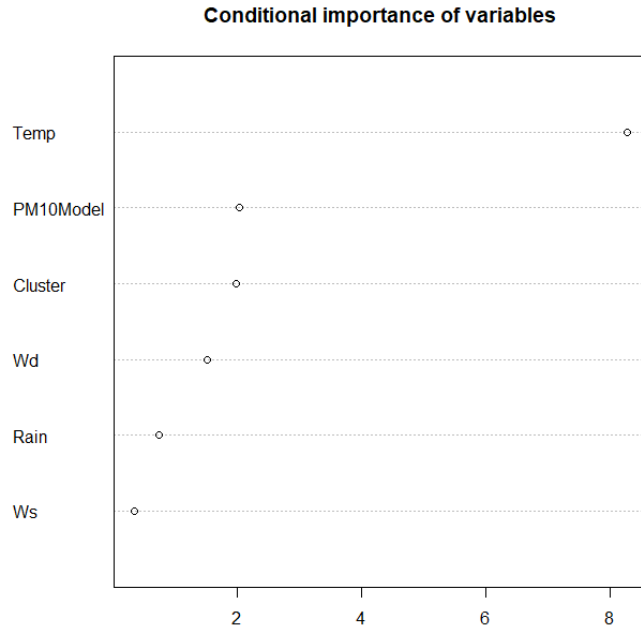
Figure 42. Conditional importance of variables about PM_{10} level in Ulsan

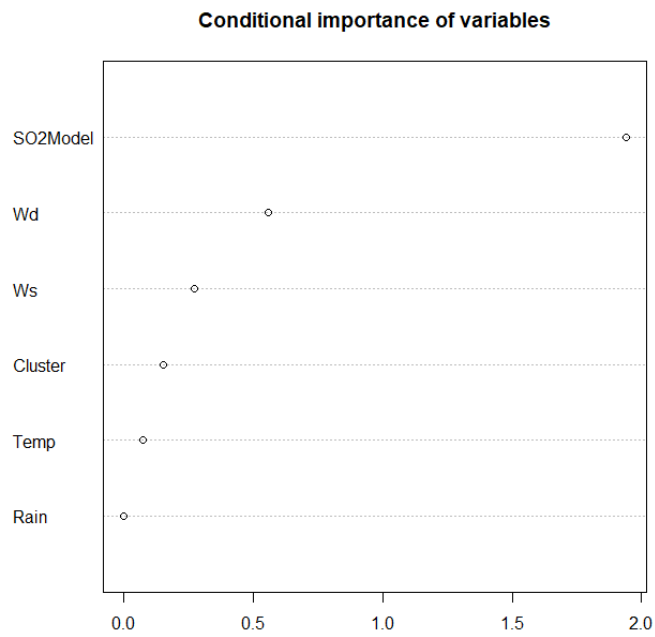**Conditional importance of variables**

Figure 43. Conditional importance of variables about SO_2 level in Ulsan
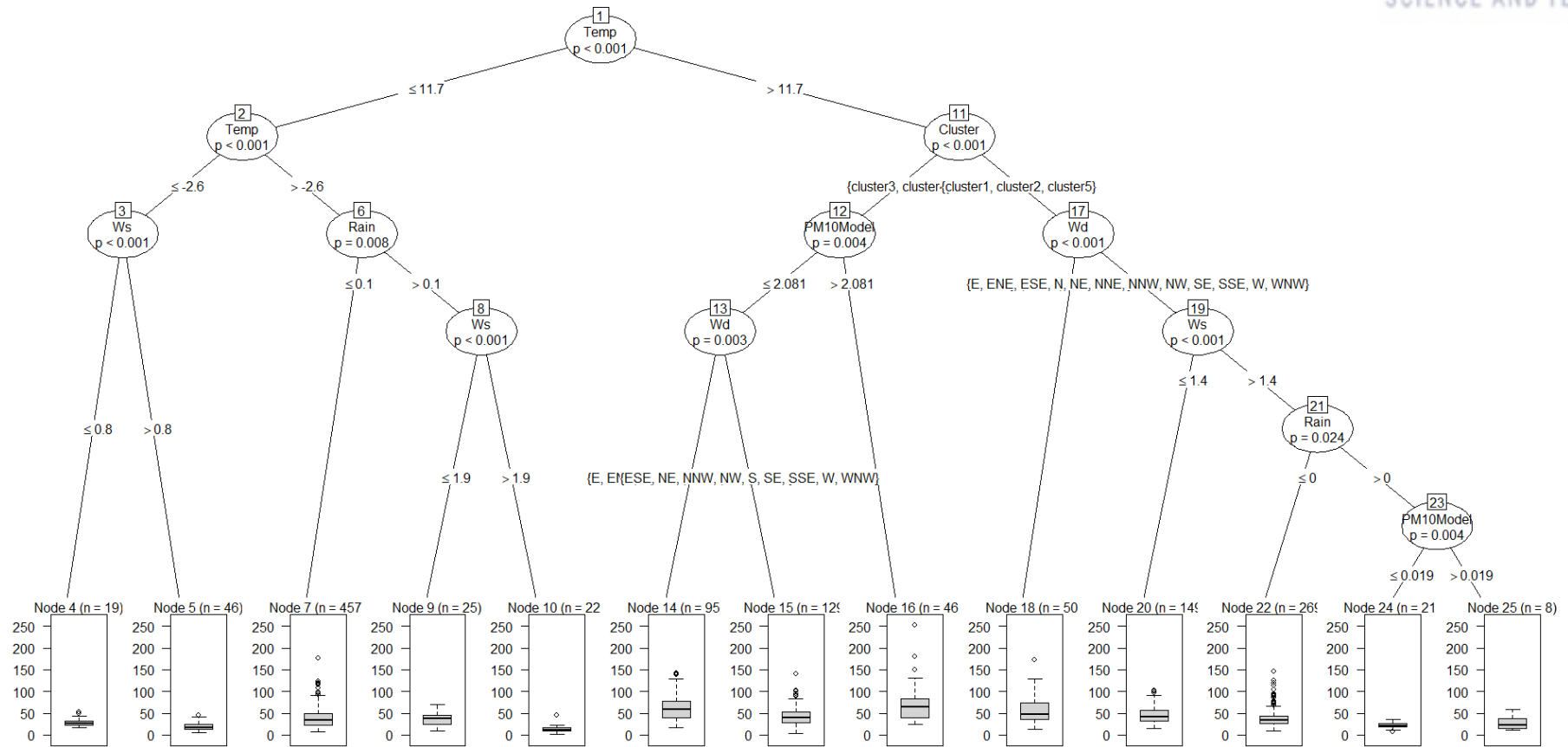
Figure 44. Conditional Interference Tree (CIT) of PM$_{10}$ level

IV. CONCLUSIONS

The conclusion can be divided two parts, interpretation of monitoring result and modeling result. In summary of monitoring part, the PM_{10} level was the highest in spring and SO_2 was in summer. Comparing with type of area, industrial, residential, and road side, the industrial area was more polluted by PM_{10} and SO_2. However, PM_{10} and SO_2 concentration was not significantly related with each other. CBPF plot showed PM10 level showed the direction of high level sources was petrochemical industrial area, surrounding effect, and other direction. On the other hands, SO_2 level showed the most of high level sources was indicated from petrochemical and non-ferrous industrial sources in industrial, residential, and road sites.

The surface wind field derived by CALMET model indicated the influence of air pollutants from industrial area to residential area was the highest in summer. PM_{10} emission affected to residential area from petrochemical area and the case of SO_2 was petrochemical and non-ferrous industrial area. The PM_{10} emission effect was low comparing monitoring level, and SO_2 emission effect was similar with monitoring level and pattern. CALPUFF result derived SO_2 level in Ulsan was influenced by point source from petrochemical and non-ferrous industrial complexes.

The backward trajectory with PSCF analysis showed the high level of PM_{10} was influenced by China during spring. In addition, cluster analysis identified the Bejing and Tenjin industrial area located in east of China was the largest potential sources among the LART effects. Shang-hai was also high potential sources next to Bejing and Tenjin industrial area. To comparing LRAT effect and local point source emission effect, CIT and RandomForeat methods were conducted. As a result, importance was similar with local point source and clusters, but other factors like temperature and precipitation were more important. That means, secondary aerosol and other local sources such as mobile sources and area sources were considered. The most important factor of SO_2 level was derived as point sources, modeling result.

In this study, using hourly data of CAPs and meteorological data, PM_{10} and SO_2 sources were identified by using modeling and statistical approach. The PM_{10} level in Ulsan was influenced by industrial emission, and LRAT from Bejing and Tenjin industrial area in China. In addition, other sources like secondary formation and mobile and area sources also affected to PM_{10} level. On the other hand, the SO_2 level was only influenced by petrochemical and non-ferrous industrial complexes. Therefore, Ulsan consider about these results to improve atmospheric environment.

REFERENCES

Alan, L.D. and Robert, D.H., 2011. CALPUFF and AERMOD model validation study in the near field: Martins creek revisited. Journal of the Air and Waste Management Association 64, 647-659.

Breiman, L., 2001. Random forests. Machine Learning. 45, 5-32.

Carslaw, D.C., Beevers, S.D., 2013. Characterising and understanding emission sources using bivariate polar plots and k-means clustering. Environmental Modelling & Software 40, 325-329.

Carslaw, D.C., Ropkins, K., 2012. openair — An R package for air quality data analysis. Environmental Modelling & Software 27–28, 52-61.

Cheung, H.-C., Wang, T., Baumann, K., Guo, H., 2005. Influence of regional pollution outflow on the concentrations of fine particulate matter and visibility in the coastal area of southern China. Atmospheric Environment 39, 6463-6474.

Chin, M., Jacob, D.J., Gardner, G.M., Foreman F, M.S., Spiro, P.A., Savoie, D.L., 1996. A global three-dimensional model of tropospheric sulfate. Journal of Geophysical Research-Atmospheres 101, 18667-18690.

Choi, E.H., Choi, K.H., Yi, S.-M., 2011. Non-methane hydrocarbons in the atmosphere of a Metropolitan city and a background site in South Korea: Sources and health risk potentials. Atmospheric Environment 45, 7563-7573.

Chung, Y.-S., 1992. On the observations of yellow sand (dust storms) in Korea. Atmospheric Environment. Part A. General Topics 26, 2743-2749.

Clarke, K., Kwon, H.-O., Choi, S.-D., 2014. Fast and reliable source identification of criteria air pollutants in an industrial city. Atmospheric Environment 95, 239-248.

Daria B., Carsten, A.S., Malgorzata, W., Maciej, K., Malgorzata, M., Justyna, K., Anetta, D.-O., 2017. Source regions of ragweed pollen arriving in south-western Poland and the influence of meteorological data on the HYSPLIT model results. Aerobiologia 33, 315-326.

Dmitry, T., Eli, S., David, M.B., 2016. Comparison of dry deposition estimates of AERMOD and CALPUFF from area sources in flat terrain. Atmospheric Environment 142, 430-432.

EPA, U., 2015. United States Environmental Protection Agency.

Gao, C., Yin, H., Ai, N., Huang, Z., 2009. Historical Analysis of SO2 Pollution Control Policies in China. Environmental Management 43, 447-457.

Goossens, D., Buck, B., 2011. Effects of wind erosion, off-road vehicular activity, atmospheric conditions and the proximity of a metropolitan area on PM10 characteristics in a recreational site. Atmospheric Environment 45, 94-107.

Han, Y.-J., Thomas, M.H., Philip K.H., Cheong, J.-P., Kim, H., Yi, S.-M., 2004. Identification of source locations for atmospheric dry deposition of heavy metals during yellow-sand events in Seoul, Korea in 1998 using hybrid receptor models. Atmospheric Environment 38, 5353-5361.

Hothorn, T., Hornik, K., Zeileis, A., 2006. Unbiased recursive partitioning: a conditional inference framework. Journal of Computational and Graphical Statistics 15, 651-674.

Hothorn, T., Hornik, K., Zeileis, A., 2017. ctree: Conditional inference trees.

Huang, R.-J., Zhang, Y., Bozzetti, C., Ho, K.-F., Cao, J.-J., Han, Y., Daellenbach, K.R., Slowik, J.G., Platt, S.M., Canonaco, F., Zotter, P., Wolf, T., Pieber, S.M., Bruns, E.A., Crippa, M., Ciarelli, G., Piazzalunga, A., Schwikowski, M., Abbaszade, G., Schnelle-Kreis, J., Zimmermann, R., An, Z., Szidat, S., Baltensperger, U., Haddad, I.E., Prevot, S.H., 2014. High secondary aerosol contribution to particulate pollution during haze events in China. Nature 514, 218.

In, H.-J., Park, S.-U., 2002. A simulation of long-range transport of Yellow sand observed in April 1998 in Korea. Atmospheric Environment 36, 4173-4187.

Itraxe, U.-T., David, C.C., 2014. Conditional bivariate probability function for source identification. Environmental Modelling & Software 59, 1-9.

Jeong, J.-H., Shon, Z.-H., Kang, M.S., Song, S.-K., Kim, Y.-K., Park, J.S., Kim, H.J., 2017. Comparison of source apportionment of PM2.5 using receptor models in the main hub port city of East Asia: Busan. Atmospheric Environment 148, 115-127.

Kim, B.-G., Park, S.-U., 2001. Transport and evolution of a winter-time Yellow sand observed in Korea. Atmospheric Environment 35, 3191-3201.

Kim, H.C., Kim, E.H., Bae, C.H., Cho, J.H., Kim, B.U., Kim, S.T., 2017. Regional contribution to particulate matter concentration in the Seoul metropolitan area, South Korea: seasonal variation and sensitivity to meteorology and emissions inventory. Atmospheric Chemistry and Physics 17, 10315-10332.

Kroll, J.H. and Seinfeld, J.H., 2008. Chemistry of secondary organic aerosol: Formation and evolution of low-volatility organics in the atmosphere. Atmospheric Environment 42, 3593-3624.

Lee, D.G., Lee, Y.-M., Jang, K.-W., Yoo, C., Kang, H.-K., Lee, J.-H., Jung, S.-W., Park, J.-M., Lee, S.B., Han, J.-S, Hong, J.-H., Lee, S.-J., 2011. Korea national emissions inventory system and 2007 air pollutant emissions. Asian Journal of Atmospheric Environment 5-4, 278-291.

Lee, G.-S., Kim, P.-R., Han, Y.-J., Thomas, M.H., Seo, Y.-S., Yi, S.-M., 2016. Atmospheric speciated mercury concentrations on an island between China and Korea: sources and transport pathways. Atmospheric Chemistry and Physics 16, 4119-4133.

Lee, Y., Choi, S., Kwon, H., Kim, C., Son, H., Ye, J., 2011. Temporal and spatial distribution of sulfur dioxide in Ulsan, Korea. J. Korean Soc. Environ. Anal 14, 24.

Leo, B., Friedman, J.H., Olshen, R.A., Stone, C.J., 1984. Classification and regression trees.

Liaw, A., Wiener, M., 2018. Breiman and Cutler's Random Forests for Classification and Regreesion.

Lim, Y.B. and Ziemann, P.J., 2005. Products and mechanism of secondary organic aerosol formation from reactions of n-Alkanes with OH radicals in the presence of NOx. Environmental Science and technology 39, 9229-9236.

Lin, C.-Y., Liu, S.C., Chou, C.C.K., Huang, S.-J., Liu, C.-M., Kuo, C.-H., Young, C.-Y., 2005. Long-range transport of aerosols and their impact on the air quality of Taiwan. Atmospheric Environment 39, 6066-6076.

Lin, T., Marie, H.-E., Karin, S., Janine, W., Peter, M., Gerd, S., 2014. Estimation of the long-range transport contribution from secondary inorganic components to urban background PM10 concentrations in south-western Sweden during 1986-2010. Atmospheric Environment 89, 93-101.

Maji, S., Ahmed, S., Siddiqui, W.A., Ghosh, S., 2017. Short term effects of criteria air pollutants on daily mortality in Delhi, India. Atmospheric Environment 150, 210-219.

Manahan, S.E., 2009. Fundamentals of Environmental Chemistry (3rd edition). CRC Press.

Robert, C.G., Alan, H.H., Sethu, R., Metropolitan-scale transport and dispersion from the New York world trade center following September 11, 2001. Part II: An application of the CALPUFF plume model. Pure and Applied Geophysics 162, 2005-2028.

Sait, C.S., Aysun, S., Thomas, M.H., Colleen, M.A., James, J.P., 2013. Atmospheric concentrations and potential sources of PCBs, PBDEs, and pesticides to Acadia National Park. Environmental Pollution 177, 116-124.

Scire, J.S., Strimaitis, D.G., Yamartino, R.J., 2000. A User's Guide for the CALPUFF dispersion model.

Score, J.S., Robe, F.R., Fernau, M.E., Yamartino, R.J., 2000. A User's Guide for the CALMET meteorological model.

Song, H.-M., Lee, D.-H., Lee, K.-S., An, S.-S., Lee, S.-H., Yang, T.-C., Kim, S.-J., Juen, H.-D., Seo, G.-Y., Do, W.-G., Cho, Y.-G., 2017. Characterization of PM10 concentration in urban Gwangju and its source identification based on cluster analysis of air mass trajectory. Journal of the Korean Society for Environmental Analysis 20, 239-251.

Stojic, A., Stojic, S.S., 2017. The innovative concept of three-dimensional hybrid receptor modeling. Atmospheric Environment 164, 216-223.

Strobl, C., Boulesteix, A.-L., Kneib, T., Augustin, T., Zeileis, A., 2008. Conditional variable importance for random forests. BMC Bioinforma. 9, 307.

Torgyn, S., Dave, L., Sunil, D., David, B., Robert, H., 2017. Decision tree and random forest models for outcome prediction in antibody incompatible kidney transplantation. Biomedical Signal Processing and Control, Article in Press.

Toshihiko, T., Itsushi, U., Teruyuki, N., Akiko, H., Itaru, S., 2002. Modeling study of long-range transport of Asian dust and anthropogenic aerosols from East Asia. Geophysical Research Letters 29, 2158.

Uria-Tellaetxe, I., Carslaw, D.C., 2014. Conditional bivariate probability function for source identification. Environmental Modelling & Software 59, 1-9.

Venables, W.N. and Smith, D.M., 2018. An Introduction to R: Notes on R: A Programming Environment for Data Analysis and Graphics.

WHO, 2013. Health effects of particulate matter.

ACKNOWLEDGEMENT

초창기 맴버였던 현진이, 놀리는거 좋아하던 지영이 등 졸업해서 지금은 없지만 좋은 추억을 남긴 EACL 졸업생 선배분들에게도 감사의 말씀을 전합니다.

실험이 필수인 우리 연구실에 맨 처음 저에게 실험을 가르쳐주고, 좋은 말씀 많이 해주며 때로는 선생님처럼, 때로는 친구처럼 정말 편안한 느낌으로 많은 걸 가르쳐주신 이윤세 선생님, 장난기 많으시고 친근하지만 실험하실 때는 진지하고 철저하신 예진 선생님, 언제나 웃으며 인사해주시고 잘 챙겨주시는 손희식 선생님, 제가 HRMS 때문에 귀찮게 자주 해서 죄송하지만 항상 절 가르쳐주시고 멋진 모습을 많이 보여주신 김철수 선생님 모두 감사드립니다. 환경분석센터가 있었기에 저도 EACL 에 들어올 수 있었습니다.

또한 연구 의외에 스트레스 받을 때나 힘들 때 옆에 있어준 진영이, 은훈이, 석태, 민규, 그 외 우리 오삐계 친구들 모두 정말 감사합니다. 육체적으로 정신적으로 힘들 때 버틴 원동력이 되어주었기에 제가 이렇게 학위를 무사히 받을 수 있었습니다.

마지막으로 한번 더 저의 가장 소중한 가족들에게 감사드립니다. 열심히 연구하여 멋진 아들, 멋지고 떳떳한 사람이 되어 행복하게 살겠습니다.

CURRICULUM VITAE

Sang-Jin Lee, M.S. student

School of Urban and Environmental Engineering, Ulsan National Institute of Science and Technology (UNIST), 100, Banyeon-ri, Eonyang-eup, Ulsan, 689-805, Korea

Tel: +82-52-217-2875, E-mail: lsjin1347@unist.ac.kr

Education

2016. 09 -	School of Urban and Environmental engineering, Ulsan National Institute of Science and Technology (UNIST), Korea (M.S.)
2010. 03 - 2016. 08	Energy and Chemical Engineering, Ulsan National Institute of Science and Technology(UNIST), Korea (B.S.)

Researcher experiences

2018.03 –	R&E project – Investigation of high concentration of particulate matters in Ulsan by using statistical and modeling method
2017.03 – 2017.09	R&E project – Source identification and spatial distribution of particulate matters in Ulsan
2016.03 – 2016.09	R&E project – Back trajectory and deposition analysis for fate of environmental pollutant in arctic site (Greenland).
2013.05 – 2016.08	Internship student of Environmental Analytical Chemistry Lab (EACL) in UNIST

Research Interests

- Monitoring of toxic chemicals associated with fine particles
- Multimedia monitoring of persistent organic pollutants (POPs)
- Source identification of criteria air pollutants(CAPs) using air-dispersion model and receptor model
- Monitoring and long-range atmospheric transport (LRAT) of POPs in polar regions

Thesis

Source identification of PM10 and SO2 in a multi-industrial city of Kora. MS thesis, Ulsan National Institute of Science and Technology (UNIST), 2018.08

Publications in Domestic Journals

[3] ung-Ho Kang∗, Heejin Hwang, Sang-Jin Lee, Sung-Deuk Choi, Je-Hyun Baek, Sang Bum Hong, Soon Do Hur, "North American boreal forest fires recorded in northwest Greenland snow" To be submitted

[2] Sang-Jin Lee, Sung-Deuk Choi∗, "Local source identification of criteria air pollutants (CAPs) in a multi-industrial city, Ulsan" To be submitted

[1] Phan Quang Thang, Seong-Joon Kim, <u>Sang-Jin Lee</u>, Jin Ye, Young-Kyo Seo, Sung-Ok Baek, Sung-Deuk Choi, "Seasonal characteristics of particulate polycyclic aromatic hydrocarbons (PAHs) in a petrochemical and oil refinery industrial area on the west coast of South Korea" Submitted

Publications in Domestic Journals (In Korean)

[1] 김성준, 박현진, <u>이상진</u>, 김창혁, 이승복, 최성득, "지리정보시스템을 활용한 서울시 유해 대기오염물질 우선순위 측정지역 선정", 한국대기환경학회지, 34(2), 223-232 (2018년 4월)

Presentation at International conferences

[8] Tuyet Nam Thi Nguyen, <u>Sang-Jin Lee</u>, Quang Tran Vuong, Sung-Deuk Choi, "Application of altitudinal potential source contribution function and concentration weighted trajectory for identifying spatial emission sources and long-range transport of PAHs", 2nd international conference Bioresources, Energy, Environment, and Materials technology (BEEM), June 10-13, 2018, Hongcheon, Korea

[7] Min-Kyu Park, Yun-Se Lee, <u>Sang-Jin Lee</u>, Leesun Kim, Yoon-Seok Chang, Sung-Deuk Choi, "Contamination characteristics of PCDD/Fs and DL-PCBs in fishery products and exposure by dietary intake of the Koreans", 2nd international conference Bioresources, Energy, Environment, and Materials technology (BEEM), June 10-13, 2018, Hongcheon, Korea

[6] Seong-Joon Kim, <u>Sang-Jin Lee</u>, Ho-Young Lee, Chang-Hyeok Kim, Seung-Bok Lee, Sung-Deuk Choi, "Atmospheric volatile organic compounds (VOCs) in the Seoul metropolitan city, South Korea: Spatial distribution, seasonal variation, and source identification", 2nd international conference Bioresources, Energy, Environment, and Materials technology (BEEM), June 10-13, 2018, Hongcheon, Korea

[5] Sung-Deuk Choi, Seong-Joon Kim, Min-Kyu Park, Hyeon-Jin Park, <u>Sang-Jin Lee</u>, Tuyet Nam Thi Nguyen, "Passive air sampling for monitoring of hazardous air pollutants (HAPs) and persistent organic pollutants (POPs)", 46th International Symposium on High Performance Liquid Phase Separations and Related Techniques, November 5-9, 2017, Jeju, Korea

[4] Seong-Joon Kim, Hyeon-Jin Park, <u>Sang-Jin Lee</u>, Chang-Hyeok Kim, Seung-Bok Lee, Sung-Deuk Choi, "Atmospheric polycyclic aromatic hydrocarbons (PAHs) in the capital city of Seoul, South Korea: spatial distribution, seasonal variation, and source identification", 36th International Symposium on Halogenated Persistent Organic Pollutants, August 20-25, 2017, Vancouver, Canada

[3] <u>Sang-Jin Lee</u>, Sung-Deuk Choi, "Source identification of criteria air pollutants (CAPs) in Ulsan, Korea", 17th IUAPPA World Clean Air Congress and 9th CAA Better Air Quality (WCAC&BAQ), August 29-September 2, 2016, Busan, Korea

[2] <u>Sang-Jin Lee</u>, Sung-Deuk Choi, 17th IUAPPA World Clean Air Congress and 9th CAA Better Air Quality (WCAC&BAQ), August 29-September 2, 2016, Busan, Korea

[1] <u>Sang-Jin Lee</u>, Sung-Deuk Choi, "Source identification of particulate matters in an industrial city", 2015 International Chemical Congress of Pacific Basin Societies (Pacifichem 2015), December 15-20, 2015, Honolulu, Hawaii

Presentation at Korean conferences

[18] 김성준, <u>이상진</u>, 이호영, 이단비, 최성득, "우선순위 선정과 모니터링을 기반으로 한 울산시 유해화학물질의 위해성평가", 한국대기환경학회 공동학술심포지움, 서울시립대학교, 2018년 5월 11일

[17] <u>이상진</u>, 박현진, 김성준, 최성득, "유해대기오염물질 측정분석과 확산모델을 이용한 울산시 미세먼지 오염특성 파악", 한국대기환경학회 공동학술심포지움, 서울시립대학교, 2018년 5월 11일

[16] <u>이상진</u>, 최성득, "대기확산모델을 이용한 울산시 배출원별 PM10 오염기여도 산정", 한국대기환경학회 추계학술대회, 대구 EXCO, 2017년 11월 9-10일

[15] 김성준, 박현진, <u>이상진</u>, 최성득, "지리정보시스템을 활용한 유해대기오염물질 측정지점 선정", 한국대기환경학회 추계학술대회, 대구 EXCO, 2017년 11월 9-10일

[14] 김성준, 박현진, <u>이상진</u>, 김창혁, 이승복, 최성득, "서울시 휘발성유기화합물의 공간분포와 오염원 추정", 한국환경분석학회 춘계학술대회, 울산과학기술원, 2017년 5월 25-26일

[13] 박현진, <u>이상진</u>, 김성준, 최성득, "울산시 도시대기측정망의 PM10과 PM2.5 상관관계 분석", 한국환경분석학회 춘계학술대회, 울산과학기술원, 2017년 5월 25-26일

[12] <u>이상진</u>, 최성득, "대기확산모델을 이용한 울산시 산업단지별 PM10 오염기여도 산정", 한국환경분석학회 춘계학술대회, 울산과학기술원, 2017년 5월 25-26일

[11] Seong-Joon Kim, Hyeon-Jin Park, <u>Sang-Jin Lee</u>, Chang-Hyuk Kim, Seung-Bok Lee, Sung-Deuk Choi, "Investigation on the spatial distribution and major sources of hazardous air pollutants (HAPs) in Seoul", 코리아 POPs 포럼 동계심포지엄, 대명비발디파크, 2017년 2월 9일

[10] <u>Sang-Jin Lee</u>, Sung-Deuk Choi, "Local source identification of criteria air pollutants (CAPs) in Ulsan, Korea", 코리아 POPs 포럼 동계심포지엄, 대명비발디파크, 2017년 2월

[9] 김성준, 박현진, <u>이상진</u>, 김창혁, 이승복, 최성득, "서울시 유해대기오염물질의 공간분포 파악을 통한 오염원 추정", 한국분석과학회 추계학술대회, 제주 메종글래드호텔, 2016년 11월 17-18일

[8] 김성준, 박현진, <u>이상진</u>, 최성득, "지리정보시스템을 이용한 서울시 유해대기오염물질 우선순위 측정지점 선정", 한국환경분석학회 추계학술대회, 제주 오션스위츠호텔, 2016년 11월 3-4일

[7] 박현진, 김성준, <u>이상진</u>, 최성득, "공간 보간법을 이용한 울산시 대기측정소의 PM10 우선순위 평가", 한국환경분석학회 추계학술대회, 제주 오션스위츠호텔, 2016년 11월 3-4일

[6] <u>이상진</u>, 강정호, 최성득, "하이브리드 수용모델을 이용한 그린란드 눈 시료의 납 오염원 추적", 한국환경분석학회 추계학술대회, 제주 오션스위츠호텔, 2016년 11월 3-4일

[5] 김성준, <u>이상진</u>, 박현진, 최성득, "위험유해물질 현장탐지 및 분석 시스템 개발", 한국위험물학회, 명지대학교, 2016년 08월 18-19일

[4] Quang Tran Vuong, Seong-Joon Kim, Hyeon-Jin Park, <u>Sang-Jin Lee</u>, Sung-Deuk Choi, "Atmospheric Monitoring of Halogenated Polycyclic Aromatic Hydrocarbons in Ulsan, Korea", 한국환경분석학회 춘계학술대회, 경주 현대호텔, 2016년 5월 26-27일

[3] 박현진, 김성준, <u>이상진</u>, 최성득, "울산지역 PM10과 PM2.5의 농도분포와 오염원 파악", 한국환경분석학회 춘계학술대회, 경주 현대호텔, 2016년 5월 26-27일

[2] 김성준, 권혜옥, <u>이상진</u>, 박현진, 최성득, "울산시 유해화학사고 가능 물질과 피해예상지역 선정", 한국분석과학회 춘계학술대회, 평창 알펜시아 리조트, 2016년 5월 19-20일

[1] 박민규, 이윤세, <u>이상진</u>, 장윤석, 최성득, "국내 소비 농산물류 중 PCDD/Fs와 DL-PCBs의 오염특성", 한국환경분석학회 추계학술대회, 제주 오션스위츠호텔 컨벤션홀, 2015년 11월 5-6일

Research projects

[11] 유해화학물질 수환경 유출 모니터링 및 유출방지 시스템 개발, 한국환경산업기술원, 2017.06~2019.12

[10] 동북아 대기오염 국가간 상호영향 공동연구(V), 국립환경과학원, 2017.05~2017.11

[9] 울산광역시 미세먼지(PM-10, PM-2.5) 오염현상에 관한 연구, 울산녹색환경지원센터, 2017.05~2017.12

[8] 울산시 미세먼지 공간분포와 오염원 파악 (R&E 과제), UNIST, 2017.04~2017.10

[7] 도시지역 우선관리 유해대기오염물질 측정망 구축 및 운영전략 연구, 한국환경산업기술원, 2016.05~2017.01

[6] 북극 환경오염추적을 위한 공기 역궤적 분석과 침적자료 해석 (R&E 과제), UNIST, 2016.04~2016.10

[5] HNS 유출사고 현장 대응기술 및 장비개발, 국민안전처, 2015.05~2019.04

[4]   생화학 및 화학재난 감시 긴급대응 기술 및 장비 개발, UNIST, 2015.03~2020.02

[3]   화학물질 사고 대응 유해화학물질 위해성 평가 기술 개발, 화학연구원,
      2014.09~2016.09

[2]   잔류성유기오염물질의 대기침적과 다매체 거동, 교육부, 2013.11~2016.10

[1]   식품 중 다이옥신, PCBs 안전관리 연구, 식약처, 2012.02~2016.11

Domestic Patents

      출원일자: 2017.08.10

      특허명칭: 대기 오염 모니터링 방법 및 대기 오염 모니터링 서버

[2]   출원번호: 10-2017-0101700

      출원인: 울산과학기술원

      발명인: 최성득, 김성준, 박현진, **이상진**

      출원일자: 2017.03.30

      특허명칭: 무인기 탑재형 기체 채취 장비

[1]   출원번호: 10-2017-0040702

      출원인: 울산과학기술원

      발명인: 최성득, 김성준, **이상진**, 박현진

Awards and Honors

[1]   한국분석학회 2015년 추계학술대회 우수포스터상 (3저자)

References

[1]   **Sung-Deuk Choi** (professor): MS supervisor

      School of Urban and Environmental Engineering, Ulsan National Institute of Science and

      Technology (UNIST), 100, Banyeon-ri, Eonyang-eup, Ulsan, 689-805, Korea

      Tel: +82-52-217-2811   Fax: +82-52-217-2809   E-mail: sdchoi@unist.ac.kr